colloids and interfaces

MDPI

*Article*

# Selective Aggregation of Fine Spodumene from Quartz with Anionic Polyacrylamide Flocculant and Calcium Activator

**Danni Luo [1,2], Wei Sung Ng [1,2,3,*] and George V. Franks [1,2,3,*]**

[1] Department of Chemical Engineering, University of Melbourne, Parkville, VIC 3010, Australia; d.luo3@student.unimelb.edu.au (D.L.); wei.ng@unimelb.edu.au (W.S.N.)
[2] Future Battery Industries Cooperative Research Centre, Bentley, WA 6102, Australia
[3] Australian Research Council Centre of Excellence for Enabling Eco-Efficient Beneficiation of Minerals, Parkville, VIC 3010, Australia
* Correspondence: gvfranks@unimelb.edu.au; Tel.: +61-03-8344-9020

**Abstract:** Fine spodumene particles are challenging to treat by froth flotation and are often discarded. An approach to recover the lithium-bearing mineral is to selectively aggregate fine spodumene into larger sizes that are amenable to recovery by flotation. This research investigated the aggregation behaviour of spodumene and the gangue minerals K-feldspar and quartz, using commercially available anionic polyacrylamide flocculants. Calcium ions were used as activators that facilitated the selective adsorption of the carboxylate groups in the anionic flocculants onto the spodumene surface. The calcium ions decreased the magnitude of the negative zeta potential and reversed the zeta potential to positive for spodumene and K-feldspar, but not for quartz, below pH 10. Calcium concentrations of 312.5 g/t enhanced the adsorption of anionic polymers onto spodumene and K-feldspar, inducing aggregation, while quartz was aggregated only above 5000 g/t. Increasing the polymer concentration increased the aggregate size for spodumene and K-feldspar, but had little effect on quartz. In situ sizing and turbidity measurements indicated the optimal conditions for spodumene aggregation were 625 g/t of calcium and 63–84 g/t of the 58% anionic-charged polyacrylamide at pH 8.5. The sedimentation results showed limited separation due to quartz entrapment in the aggregates. Anionic polyacrylamide flocculants with calcium activators can aggregate fine spodumene particles.

**Keywords:** selective flocculation; spodumene; anionic polyacrylamide; calcium activation



Academic Editor: Margaritis Kostoglou

Received: 2 May 2025
Revised: 5 June 2025
Accepted: 6 June 2025
Published: 11 June 2025

**Citation:** Luo, D.; Ng, W.S.; Franks, G.V. Selective Aggregation of Fine Spodumene from Quartz with Anionic Polyacrylamide Flocculant and Calcium Activator. *Colloids Interfaces* **2025**, *9*, 36. https://doi.org/10.3390/colloids9030036



## 1. Introduction

As the primary hard-rock source of lithium, spodumene ($LiAlSi_2O_6$) plays a critical role in global lithium supply chains, which underpin technologies, such as electric vehicles, portable electronics, and renewable energy storage systems [1–4]. The urgency to transition toward sustainable energy sources has intensified the demand for lithium, placing spodumene processing at the centre of strategic efforts to secure critical mineral resources [5–7].

Froth flotation is the most widely used method for concentrating spodumene [8,9]. Declining ore grades necessitate fine grinding, but particles below 20 μm are typically unrecoverable due to the low particle–bubble collision probability, high reagent dose requirements, and surface sliming effects [10–16]. These slimes are often removed prior to flotation to avoid any negative impact on flotation, resulting in substantial lithium losses [17]. Improving the recovery of fine spodumene could therefore deliver significant economic benefits.

The presence of gangue minerals, in the form of quartz and feldspar, are difficult to separate from spodumene. The effectiveness of froth flotation is limited due to the difficulty of distinguishing between the surface of these minerals and that of spodumene, owing to their similar surface properties, including similar isoelectric points [8,18,19]. Despite extensive research into alternative methods and chemistries for improving selectivity, fatty acids, such as sodium oleate (NaOL), are still the most commonly used primary collectors, although they exhibit limited selectivity for spodumene flotation from some of the gangue minerals [8,18,19].

To improve the selectivity and flotation performance, metal ions, including iron, magnesium, and calcium, play a pivotal role in enhancing the selective attachment of sodium oleate to spodumene surfaces, significantly improving the flotation efficiency [20–26]. This enhancement is attributed to the ability of metal ions to activate the spodumene surface and act as a bridge between the negatively charged spodumene surface and the carboxylate group of the anionic surfactant, NaOL, thereby increasing the hydrophobicity of the mineral and facilitating its collection by froth flotation [22]. NaOL is thought to form mono- and di-oleate complexes with calcium and magnesium ions, which adsorb to the spodumene surface, helping to improve the selective flotation of spodumene [21,22].

Flocculation–flotation is a method for recovering fine particles by selectively aggregating these particles into sizes conducive to flotation [27,28]. This process leverages high-molecular-weight polymers, such as polyacrylamide-based flocculants, for the selective binding and aggregation of the target mineral particles, thus forming larger aggregates that are easier to attach to bubbles [29]. Some earlier works investigated the use of temperature-responsive polymers, such as poly(N-isopropylacrylamide) (PNIPAM), to aggregate and float fine minerals, such as hematite and chalcopyrite [30–32], and were followed by studies which explored the potential of using conventional, commercial reagents for the selective aggregation and flotation of minerals, such as hematite [33,34].

There remains a notable research gap in applying these techniques specifically to the recovery of fine spodumene particles. We believe it is possible to use commercially available flocculants with a selective affinity for fine spodumene particles to efficiently aggregate them into larger aggregates, facilitating their separation from fine silica and possibly from K-feldspar particles during the froth flotation process. Only a single study on flocculation–flotation has been conducted, which applied low-molecular-weight collectors to impart shear aggregation [35] rather than high-molecular-weight polymeric flocculants known to produce larger, stronger flocs.

This study aims to contribute to the field by developing a practical and cost-effective solution to a longstanding problem in spodumene processing: the use of commercially available flocculants to selectively aggregate only fine spodumene particles from quartz and K-feldspar. One potential approach is the use of anionic polyacrylamide (PAM), which is partially hydrolysed to introduce carboxylate groups (-$COO^-$) along the polymer chain. These carboxylates are expected to have a similar interaction with the spodumene surface as that of sodium oleate (NaOL), as they both contain a negatively charged carboxylate group (-$COO^-$), facilitating the selective attachment of carboxylate functional reagents onto the spodumene surface using calcium as the activator [36,37].

Several papers have demonstrated that metal ions can influence the flocculation of other types of mineral particles with anionic PAM [38–40]. Anionic PAM is also expected to be a poor flocculant for the typical gangue minerals in spodumene treatments, such as quartz and K-feldspar, as the gangue is expected to possess a negative surface charge under typical processing conditions. However, there is little information available on the selective aggregation of spodumene over typical gangue minerals, such as quartz and K-feldspar, through the use of conventional flocculants either with or without calcium as the activator.

The objective of this study is to investigate the conditions in which spodumene can be aggregated by anionic polyacrylamide and calcium without aggregating quartz or feldspar. The effect of the calcium concentration, polymer concentration, pH levels, polymer charge, and polymer molecular weight on the aggregation behaviour of spodumene, quartz, and K-feldspar are investigated. The zeta potentials of the mineral surfaces in the absence and presence of calcium are examined, along with the adsorption isotherms of calcium and anionic PAM onto the mineral surfaces. The aggregation behaviour is characterised by measuring the turbidity of the supernatant after sedimentation of the solids, as well as with in situ particle imaging and sizing to measure the aggregate sizes. Subsequently, the sedimentation separation of spodumene from quartz is investigated through selective aggregation under the optimal conditions for spodumene.

## 2. Materials and Methods

### *2.1. Materials*

The spodumene ($LiAlSi_2O_6$) (BA830, >95% purity, -325 mesh) powders and K-feldspar ($KAlSi_3O_8$) (BA350, >90% purity) powders were sourced from Walker Ceramics Australia. The quartz ($SiO_2$) was sourced from Unimin Australia Limited (400G, 99.5% purity). The materials were used as received without any further pretreatment. The mineral samples, including spodumene, K-feldspar, and quartz, were characterised to confirm their phase purity and identity. An X-ray diffraction (XRD) analysis was conducted using a Bruker D8 Advance Powder Diffractometer equipped with a Cu K$\alpha$ source ($\lambda$ = 1.5406 Å), operating at 40 kV and 40 mA. The diffraction patterns were collected over a 2$\theta$ range of 5°–90°, with a step size of 0.02° and a scan speed of 1°/min. The XRD results, presented in Appendix A.1, Figure A1, confirm that the samples were of high purity and corresponded to their expected mineral phases. Additionally, their chemical compositions were verified by peroxide fusion followed by inductively coupled plasma–optical emission spectrometry (ICP-OES). The chemical compositions determined by ICP-OES are provided in Appendix A.2, Table A1 and further verify the elemental content of the spodumene, K-feldspar, and quartz samples.

The particle size distributions were measured by laser light scattering with a Malvern Mastersizer 3000. The results are presented in Appendix A.3, Figure A2. Furthermore, the size and morphology of the particles were investigated using a scanning electron microscope (SEM). Conductive carbon adhesive was used to affix the spodumene, K-feldspar, and quartz samples, which were then placed in a Hitachi FlexSEM scanning electron microscope. The SEM images are presented in Appendix A.3, Figure A3. The working distance was 6.07 mm, and the instrument was operated at 20.0 kV under a vacuum. Potassium chloride (KCl; AR grade, >99% purity) was used as received from Chem-Supply. Sodium hydroxide (NaOH; AR grade, >99% purity) was used without purification from Merck. Calcium chloride ($CaCl_2.2H_2O$; >99% purity) was purchased from Chem-Supply and prepared as a stock solution prior to use.

The flocculants utilised in the experiments are listed in Table 1. The polymers were polyacrylamide-based flocculants with varying degrees of hydrolysis to produce carboxylic acid functionality. Cyfloc A150 (Syensqo, Stamford, CT, USA) was used for the adsorption isotherms and turbidity studies, as well as for the investigations on the effect of the polymer concentration and calcium concentration on the aggregate size. A series of other Cyfloc polymers of similar molecular weight were used to investigate the effect of the polymer charge on the aggregate size. The series of AN934 (SNF Australia, Lara, VIC, Australia) polymers with varying molecular weights were used to investigate the effect of the polymer molecular weight on the aggregate size. For all the studies, the polymers were prepared as a 0.01 wt% solution in 0.01 M KCl as a background electrolyte in reverse osmosis (RO) water and mixed for at least 6 h before being added to the suspensions.

**Table 1.** Details of anionic polyacrylamides used in this work.

| Polymer | Charge Density | Molecular Weight (MDa) | Manufacturer |
|---|---|---|---|
| Cyfloc A100 | 6.4% | 10–15 | Syensqo |
| Cyfloc A130 | 30% | 10–15 | Syensqo |
| Cyfloc A150 | 58% | 10–15 | Syensqo |
| Cyfloc N100 | <2% | 10–15 | Syensqo |
| AN934 BPM | 30% | 6 | SNF |
| AN934 | 30% | 11–14 | SNF |
| AN934 VHM | 30% | 16.5–22.5 | SNF |

### *2.2. Methods*

#### 2.2.1. Zeta Potential

The zeta potential of the mineral particles, including spodumene, K-feldspar, and quartz, was evaluated using a Colloidal Dynamics ZetaProbe instrument. This instrument uses the electro-acoustic method to measure the zeta potential of concentrated suspensions. The suspensions contained 3.0 wt% of particles, containing varying concentrations of calcium (added as $CaCl_2$) and a 0.01 M solution of KCl in RO water. The solutions were initially prepared under alkaline conditions and subsequently titrated using an acid solution, facilitating a series of zeta potential measurements across a pH range of 2 to 11. Three measurements were taken for spodumene in the absence of Ca(II), and two measurements were taken for K-feldspar and quartz in the absence of Ca(II) to test the reproducibility of the results. These are shown in Figure A4 in the Appendix A.4.

#### 2.2.2. Adsorption of Calcium: Inductively Coupled Plasma (ICP)

The adsorption of calcium onto the mineral particles' surfaces was determined by measuring the difference between the calcium added to the suspension and that remaining in the suspension after adsorption onto the mineral surfaces. The calcium concentration in the solutions was measured by inductively coupled plasma. The spodumene, K-feldspar, and quartz samples were prepared at a concentration of 1 wt% in 10 mL of 0.01 M KCl solution, with varying concentrations of calcium ions ranging from 0 to 100 ppm, corresponding to 0 g/t to 10,000 g/t. After the addition of the calcium ions and 30 min of mixing, the samples were centrifuged at 3750 rpm for 40 min. The supernatant was then collected and diluted tenfold for the subsequent analysis.

The equilibrium concentration of the calcium ions remaining in the solution after adsorption was determined using an inductively coupled plasma–optical emission spectrometer (Varian 720-ES ICP-OES, Macquarie Park, NSW, Australia). A calibration curve was generated by measuring the known concentrations of the calcium ions, which was then used to estimate the remaining calcium ions in the supernatant. These data enabled the determination of the quantity of calcium ions adsorbed onto the minerals. The measurements were carried out at both pH 8.5 and 10.5. The measurements were repeated two or three times, as shown in Figure A5 in the Appendix A.5, to show reproducibility.

The adsorbed amount of calcium ions, expressed in mg/g, was converted to an adsorbed amount per surface area ($mg/m^2$) using the specific surface area ($m^2/g$) of the adsorbents. The surface areas of the primary particles of spodumene, K-feldspar, and quartz, determined using Malvern Mastersizer 3000 laser light scattering particle size measurements, were 0.36, 0.22, and 0.22 $m^2/g$, respectively.

#### 2.2.3. Adsorption Isotherms of Polymers: Total Organic Carbon (TOC)

The adsorption isotherms for the polymer flocculants on the mineral surfaces were determined by the depletion method. The polymer was allowed to adsorb and the amount

remaining in the solution was determined. The difference between the amount added and the amount remaining in the solution after adsorption was the adsorbed amount. To obtain the adsorption isotherm curves of the polymer A150 onto the surfaces of the different minerals (spodumene, K-feldspar, and quartz) and in the presence of calcium, 30 mL suspensions of 1 wt% mineral were first prepared using 0.01 M KCl and varying concentrations of calcium ions (between 0 g/t and 20,000 g/t, corresponding to between 0 M and 5 M) under two different pH conditions (pH 8.5 and pH 10.5). Subsequently, varying amounts of the polymer, ranging from 0 ppm to 400 ppm (corresponding to 0 g/t and 40,000 g/t), were introduced into the suspension. The mixtures were then left on a roller for a period of 6 h prior to centrifugation. The samples were centrifuged at 3750 rpm for 40 min, after which the supernatant was collected for analysis.

A total organic carbon (TOC) analysis was used to determine the equilibrium amount of the polymer remaining in the solution after adsorption. The TOC of the polymeric flocculant in the solution was measured with a Shimadzu TOC-V analyser. First, a calibration curve was made by measuring the TOC value of known-concentration polymer solutions. This calibration curve was used to estimate the quantity of the polymer (as the source of organic carbon) remaining in the supernatant. These data allowed for the determination of the quantity of the polymer adsorbed by the various minerals at different calcium concentrations and pH levels by their difference. The Langmuir isotherm model was fit to the experimental data. The adsorbed amount in mg/g could be converted to an adsorbed amount per surface area (mg/m$^2$) using the surface area (m$^2$/g) of the adsorbate. The surface areas of the primary particles of spodumene, K-feldspar, and quartz, determined from the Malvern Mastersizer 3000 laser light scattering particle size measurements were 0.36, 0.22, and 0.22 m$^2$/g, respectively.

The experiments for each calcium concentration were performed three times, with each repeat containing four to five points. The data presented in the results Section 2 are a combination of the measurements from at least 2 different experiments. Appendix A.6, Figure A6 includes data from 3 different experiments and the predicted Langmuir fitting based on the 95% confidence interval, including all 3 measurements, to demonstrate the high accuracy of the confidence interval. The raw data, with each individual experiment identified, are presented in Figure A6 in the Appendix A.6. Appendix A.7, Figure A7 expresses the adsorbed amount in units of mg/g. Appendix A.8, Figure A8 shows the adsorbed amounts in unit mmol/m$^2$.

#### 2.2.4. Aggregation (Flocculation) Procedure

The flocculation procedure entailed the use of 475 mL of a 1.0 wt% suspension of spodumene, K-feldspar, or quartz in a 0.01 M KCl solution. A 500 mL flat-bottomed glass beaker served as the reactor and was fitted with four stainless-steel baffles, as described in detail elsewhere [41,42]. The mixing process was conducted using a six-bladed stainless-steel Rushton impeller, connected to a Heidolph RZR 2020 mechanical overhead stirrer, which allows for speed variation. The impeller utilised in this study was characterised by the following dimensions: It had a diameter of 41.3 mm. The blades of the impeller, each with a length of 10.4 mm, were 1.55 mm thick. The diameter of the impeller's central disk measured 31.7 mm. The overall thickness of the impeller was 1.85 mm, and the width of the blades was 8.7 mm. The position of the impeller was maintained at one-fifth of the depth of the suspension, which optimised the motion of the suspension.

A rotational speed of 500 rpm was selected to provide the system with a shear rate similar to that found in industrial mechanical flotation cells [29,41,42]. The effective shear rate was determined to be approximately 1170 s$^{-1}$ [43]. This rate was sufficient to continuously circulate the aggregates, leading to the formation of large flocs. The pH of the suspension

was modified prior to the addition of the reagents to be either 8.5 or 10.5. The suspension was mixed for 5 min before the polymer was added; then, after the polymer addition, the suspension was mixed for 5 min while the aggregation was monitored. Several conditions were repeated two or three times, and a selection of these repeated conditions is shown in Appendix A.9, Figure A9. The results were consistent across the repeats.

#### 2.2.5. Aggregate Size Imaging and Measurement

The aggregate size imaging and measurements were conducted using a Blaze Metrics 900 probe, which is specially designed to track the changes in aggregate size during the flocculation procedure described above. The pH of the suspension was adjusted to either 8.5 or 10.5 depending on the set of studies. The Blaze probe was submersed in the aggregation vessel, as described elsewhere [41,42], to enable the in situ measurement of the aggregate size as a function of time for various combinations of polymer dose and calcium addition. The probe used a short-pulse laser light to illuminate the suspension and capture a photographic image of the particles and aggregates. The probe then used real-time image processing to determine the Image-Derived Chord Length Distributions (ID-CLD). The chord length is a measure of the length of a circular chord intersecting an object's perimeter, and is frequently used as a proxy for particle size, and the relationship between the chord length and size has been well established in the previous literature using a Focused Beam Reflectance Measurement (FBRM) apparatus [44,45].

The probe captured 58 images per second and calculated a running average of the chord length distribution from these images. The data are presented as both unweighted chord length distributions and cube-weighted distributions. The unweighted distributions are based on the number of chords measured at each length and are helpful in monitoring changes in smaller particles and aggregate populations. The cube-weighted distributions are determined by multiplying the measured counts by the cube of the length, which is more closely associated with the volume particle size distributions usually reported by particle size measurement devices. Several conditions were repeated two or three times, and the results were similar. A selection of these repeated conditions is shown in Appendix A.9, Figure A9. The results were consistent across repeats.

#### 2.2.6. Turbidity Measurement

The turbidity measurements were conducted using a HACH model 2100N turbidimeter, Dandenong South, VIC, Australia, following the flocculation procedure described above. After stirring for 5 min following the addition of the polymer, the stirring ceased, allowing the suspension to settle undisturbed for a period of 2 min. After this settling period, the supernatant was sampled approximately 2 cm below the surface, and the turbidity was measured. For the turbidity measurements, two or three measurements were taken for certain conditions to demonstrate reproducibility, and the average was reported. An example of the variability in the measurements is shown in the Appendix A.14, (Table A2).

#### 2.2.7. Sedimentation Experiments

The spodumene and quartz mixtures were prepared at a 3:7 weight ratio of spodumene to quartz in two suspension concentrations, 10 wt% and 5 wt%, each in 475 mL of distilled water. For the 10 wt% suspension, 14.25 g of spodumene and 33.25 g of quartz were used, and for the 5 wt% suspension, 7.13 g of spodumene and 16.63 g of quartz were used. The suspensions were aggregated in the reactor, as described in Section 2.2.4 above, and then allowed to settle. Table 2 shows a matrix of the experiments conducted. The solids concentration, mixing time, and sedimentation time were varied in order to understand their influence on the separation. After settling, the sediments and supernatants were separated, dried, and analysed using X-ray fluorescence (XRF) to determine the content

of spodumene and quartz. The XRF used was a Bruker S2 Puma X-ray Fluorescence (XRF) Spectrometer, Preston, VIC, Australia. Since XRF cannot directly detect Li, Al was used to determine the spodumene concentration. A mixture of spodumene and quartz in different ratios was used to generate a calibration curve for the Al (%), as shown in Figure A10 in the Appendix A.10. The Al content was then used to determine the amount of spodumene present in the sample. A sample calculation is included in the Appendix A.10. The recovery and grade of the spodumene in the sediments and supernatants were then calculated. Experimental conditions 1 and 2 were repeated three times. The average and standard deviation were calculated and plotted, and the error bars represent the 95% confidence interval.

**Table 2.** Conditions of each sedimentation experiment conducted.

| Experiment | Solids Concentration | Composition * | Mixing Time | Settling Time |
|---|---|---|---|---|
| 1 | 10 wt% | No polymer<br>No calcium | 5 min | 2 min |
| 2 | 10 wt% | 42 g/t polymer<br>625 g/t calcium | 5 min | 2 min |
| 3 | 5 wt% | 42 g/t polymer<br>625 g/t calcium | 5 min | 2 min |
| 4 | 10 wt% | 42 g/t polymer<br>625 g/t calcium | 2 min | 2 min |
| 5 | 10 wt% | 42 g/t polymer<br>625 g/t calcium | 5 min | 1 min |

* g/t refers to the number of grams of polymer or calcium ions per tonne of total solids.

## 3. Results and Discussion

### *3.1. Mineral Surface Properties*

#### 3.1.1. Particle Size Characterisation

The particle size distributions measured with a Malvern Mastersizer 3000 are shown in the Appendix A.3 as Figure A2, and the median particle sizes $d_{50}$ of spodumene, K-feldspar, and quartz were 21 µm, 21 µm, and 9 µm, respectively. The $d_{80}$ of spodumene, K-feldspar, and quartz were 39 µm, 50 µm, and 22 µm, respectively. The shape of the particles and a further confirmation of the particle size were observed by SEM and are presented in Figure A3 in the Appendix A.3. It can be seen in Figure A3 that the spodumene appears to have a blockier shape than the K-feldspar and quartz and expresses cleavage planes. The spodumene appears the least like a sphere, with an elongated structure and a higher aspect ratio.

#### 3.1.2. Zeta Potential Measurements

The zeta potential measurements for spodumene, K-feldspar, and quartz are shown in Figure 1. The reproducibility of the measurements is about ±5 mV, as shown in Figure A4 in the Appendix A.4, for the measurements of spodumene, K-feldspar, and quartz without added calcium. Spodumene is a silicate mineral which is reported to have an isoelectric point (IEP) ranging from 2.5 to 3 [21–23], which is consistent with our results of about pH 3.5. The zeta potential of K-feldspar, as reported in the literature, is somewhat different from the measurements presented here. While the trend is similar, the magnitude of the zeta potentials of our K-feldspar is not as large as the reported values, which range from −20 to −40 mV [46]. The zeta potentials of quartz presented here are consistent with the literature, except at a low pH, where the results presented here remain negative rather than showing an isoelectric point at about pH 2 [47–49]. Some other literature has also reported quartz with an isoelectric point below pH 2 [50]. These slight differences are not unusual, as minerals from different sources have slight differences in their surface chemistries, resulting in a range of surface-charging behaviours.

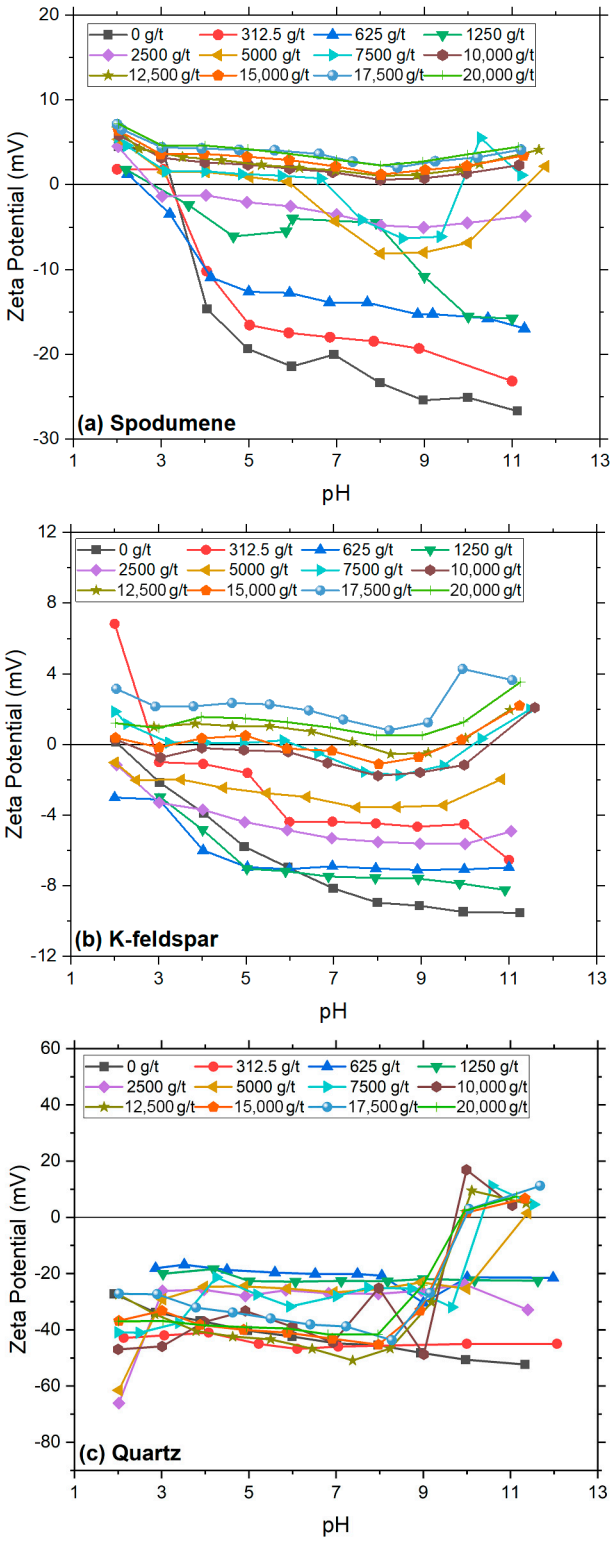


**Figure 1.** Zeta potentials of spodumene (**a**), K-feldspar (**b**), and quartz (**c**) in absence and presence of calcium, from 312.5 g/t to 20,000 g/t in 0.01 M KCl. Repeats of measurements in absence of Ca(II) are included in Figure A4. Only 1 data set is shown in this figure to avoid excessive crowding.

Upon the addition of calcium, the zeta potential of the spodumene shifted towards positive values, stabilising after the addition of 10,000 g/t of calcium, suggesting the saturated adsorption of calcium onto the spodumene. The adsorption was mainly due to the electrostatic attraction between the calcium cations ($Ca^{2+}$ and $CaOH^{+}$ above pH 10) and the negatively charged surface sites on the spodumene [51]. (The speciation of Ca(II) as a

function of pH is described in the Appendix A.11.) The zeta potential results at 5000 g/t of calcium are similar to those in the literature that used 4000 g/t of calcium ions, where the zeta potential decreased from pH 2 to 8 and then increased from pH 8 to 12 [22]. This is because the dissolved calcium ($Ca(II)_{aq}$) exists as $Ca^{2+}$ ions from pH 2 to 8 [52]. With an increasing pH, the concentration of $Ca^{2+}$ ions in a solution decreases. When the pH is above 10, the concentration of $CaOH^+$ increases, while $Ca(II)_{aq}$ are predominantly in the form of $Ca(OH)_2$ in a solution and precipitate onto solid surfaces at a pH about 12 [52]. The surface of the spodumene became predominantly positive when the calcium concentrations were above about 7500 to 10,000 g/t.

For K-feldspar, as depicted in Figure 1b, the magnitude of the zeta potential without calcium was lower than that for spodumene, with the isoelectric point occurring at a pH of approximately 2.5. The introduction of calcium ions led to a gradual increase in the zeta potential, achieving a consistently positive zeta potential with the addition of 10,000 to 12,000 g/t or more of calcium, similar to spodumene. There was little further increase in the zeta potential with increased concentrations of calcium. The similar behaviour of K-feldspar to spodumene may make it difficult to find conditions to selectively adsorb only polymers onto the spodumene surface but not K-feldspar.

The zeta potential behaviour of quartz, shown in Figure 1c, exhibited more complex characteristics. In the absence of calcium, the magnitude of the zeta potential gradually increased, from about −30 to −50 mV, as the pH increased from 2 to 12. These results are consistent with previous measurements on the same powder [50], as well as the other literature [49] which has shown quartz's IEP below pH 2. The addition of calcium resulted in the zeta potential fluctuating between about −40 mV and −20 mV for a pH below about 9, rather than forming a consistent trend. Notably, above a pH of approximately 10, the addition of calcium resulted in a positive zeta potential at concentrations above about 5000 to 7500 g/t. The sudden reversal of the zeta potential from negative to positive above pH 9 could be attributed to the adsorption of the hydroxy complex $CaOH^+$. This likely occurred through hydrogen bonding or water-forming reactions, coupled with the deprotonation of part of the silanol group (Si–OH) to form silanolate ($Si–O^-$) on the solid surface, and the surface precipitation of $Ca(OH)_2$ [38,52–54]. The precipitated $Ca(OH)_2$, having a point of zero charge above pH 12, imparted a positive potential to the surface, accounting for the observed positive zeta potential above pH 9 [55]. The trend observed in this study when the calcium concentration exceeded 5000 to 7500 g/t is consistent with the zeta potentials seen in previous research, which involved around an equivalent 40,000 g/t of calcium ions [56]. Overall, these zeta potential findings imply that a pH range between 6 and 9 is likely to be more conducive for the selective adsorption of NaOL or anionic PAM onto spodumene rather than quartz, compared to a pH value greater than 10. These results indicate that it should be relatively easy to avoid aggregating quartz under conditions suitable for aggregating spodumene. It will be more challenging to selectively aggregate spodumene without aggregating K-feldspar.

The observed differences in the surface electrical behaviour among spodumene, K-feldspar, and quartz in response to Ca(II) can be attributed to variations in their surface chemistry and crystal structures [57,58]. Spodumene and K-feldspar are both aluminosilicates, but differ in their structures and surfaces [59], which influence their interaction with Ca(II). Spodumene has Li in its structure and has more Al surface sites at a pH around 8 [60], which might promote a stronger interaction with $CaOH^+$ and a more rapid charge reversal. K-feldspar, while chemically similar, has fewer Al surface sites [61], requiring higher Ca(II) concentrations to reach comparable zeta potential changes. In contrast, quartz has a silanol surface (Si–OH) that remains highly negatively charged even in the presence of Ca(II), unless the pH is raised above 10, at which point deprotonation and precipitation

of $Ca(OH)_2$ can lead to sudden zeta potential reversal, as discussed above. These fundamental differences explain why spodumene and K-feldspar respond more readily to Ca(II) activation than quartz, and why selective flocculation conditions favour spodumene and K-feldspar over quartz at a moderate pH.

### 3.1.3. Adsorption Isotherms of Calcium

The adsorption isotherms of the calcium ions on spodumene, K-feldspar, and quartz at a pH of 8.5 and pH of 10.5 are shown in Figure 2a,b. The adsorbed amount of calcium ($mg/m^2$) is plotted against the equilibrium concentration of calcium in the supernatant (mg/L). The lines are drawn to guide the eye. The measurements were repeated three times. All the results for the multiple experiments are shown in Figure 2. The results of each individual experiment are included in the Appendix A.5, Figure A5.

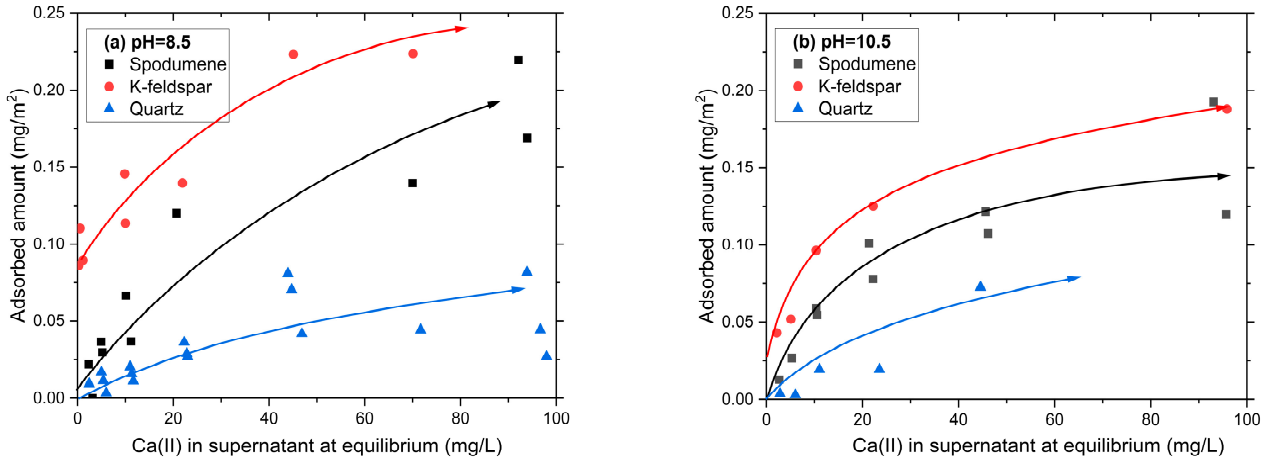


**Figure 2.** (**a**) The adsorption isotherms of calcium at pH 8.5 on the different minerals; (**b**) the adsorption isotherms of calcium at pH 10.5 on the different minerals (the lines are drawn to guide the eye). The data are combined from multiple experiments. The individual experiments are presented in the Appendix A.5, Figure A5.

At pH 8.5, the K-feldspar exhibited the highest adsorption capacity, followed by spodumene and quartz. This differs from the adsorption amounts of calcium reported on these minerals at pH 7, where the literature indicates a higher adsorption onto spodumene, followed by quartz, and then feldspar [62]. The adsorption isotherms of the calcium ions on spodumene, K-feldspar, and quartz at a pH of 10.5 are shown in Figure 2b. At pH 10.5, K-feldspar continued to exhibit a higher adsorption capacity than spodumene and quartz. The adsorption onto K-feldspar and spodumene decreased slightly at pH 10.5 compared to 8.5, while appearing to increase slightly onto quartz. The increase onto quartz found here at pH 10.5 is perhaps slightly less than expected from reports in the literature [63–66].

The adsorption capacity of calcium onto spodumene, K-feldspar, and quartz is pH-dependent. From pH 8.5 to 10.5, the species distribution of $Ca(II)_{aq}$ changes, resulting in 100 times more $Ca(OH)^+$ and $Ca(OH)_2(aq)$, while the concentration of $Ca^{2+}$ remains unchanged [62]. This change in species distribution might be the reason for the decreased efficiency of calcium adsorption onto the surfaces of the K-feldspar and spodumene as the pH was increased from 8.5 to 10.5. At pH 8.5, K-feldspar showed the highest adsorption capacity, and it continued to exhibit the highest adsorption capacity at pH 10.5. The high adsorption of $Ca(II)_{aq}$ onto K-feldspar may make it difficult to selectively adsorb polymers onto spodumene but not K-feldspar. Quartz consistently showed the lowest adsorption capacity at both pH levels.

#### 3.1.4. Adsorption Isotherms of Polymer

Figure 3a–f depict the adsorption profiles of the 58% anionic polyacrylamide (A150) onto spodumene, K-feldspar, and quartz at pH values of 8.5 and 10.5. The adsorbed amounts (mg/m$^2$) are presented as a function of the polymer concentration in the supernatant at equilibrium (mg/L) because this is the thermodynamic relationship. In addition, the results are plotted as mg/g vs. mg/L and mmol/m$^2$ vs. mmol/L in Figures A7 and A8. Figure 3a shows a monotonic increase in polymer adsorption with polymer concentration that can be modelled using the Langmuir isotherm for spodumene at pH 8.5. A plateau in adsorption is observed at higher polymer concentrations, characteristic of monolayer adsorption, beyond which further increases in the polymer concentration result in no significant change in adsorption. This also suggests a finite number of available adsorption sites, consistent with the Langmuir adsorption behaviour. Increasing the calcium concentration increases the adsorbed amount of polymer, suggesting that the calcium facilitates anionic polymer adsorption. As shown in Figure 3d, at pH 10.5, there is a slight decrease in the adsorption of the polymer onto the spodumene without calcium, but a marked increase in the polymer adsorption capacity onto spodumene for increased calcium concentrations compared to pH 8.5. At a higher pH, there is more $CaOH^+$ in the solution than at pH 8.5. Also, a higher deprotonation of the surface sites leads to an increased negative surface charge and, thus, the better interaction of $CaOH^+$ with the surface. The K-feldspar behaves like the spodumene, although the adsorption is a bit stronger in all the cases, as shown in Figure 3b,d. This may make it difficult to selectively aggregate spodumene from K-feldspar.

Figure 3c,f illustrate the adsorption characteristics of the polymer onto the quartz surfaces at pH 8.5 and 10.5, respectively. In Figure 3c, at pH 8.5, the adsorbed amount is significantly less compared to the spodumene and K-feldspar under the same conditions, consistent with the zeta potential results (Figure 1), showing that quartz is negatively charged, which inhibits the adsorption of the anionic polymer. Even with calcium present, it is difficult for the anionic polymer to adsorb onto quartz. Figure 3f, depicting quartz at pH 10.5, shows a similar trend but with a notable increase in adsorption. This indicates that the polymer adsorption onto quartz is enhanced at higher pH levels, but only with calcium concentrations of around 10,000 g/t. At low calcium concentrations, calcium ions do not effectively bind to quartz. Since quartz has a negative surface charge, it is difficult for the negatively charged polymer to adsorb onto it. However, with higher calcium concentrations (10,000 g/t) at pH 10.5, the surface becomes positive, as shown in the zeta potential results (Figure 1). This is likely due to the increased concentration of $Ca(OH)^+$, which adsorbs onto the quartz surface [52,56,65,67], consistent with the previous calcium isotherm results presented in Figure 2. This results in a fourfold increase in the polymer adsorption.

A higher pH with a higher calcium concentration boosts polymer adsorption onto quartz, since $Ca(OH)^+$ facilitates anionic polymer adsorption in a similar way that it facilitates NaOL adsorption. This result is consistent with the research showing that calcium increases NaOL adsorption onto quartz when the pH is above 9. Below a pH of 9, the effect is not obvious [66]. These adsorption results are consistent with the previous zeta potential measurements (Figure 1). When the pH is above 9 and the calcium concentration is higher than 5000 g/t, the surface of quartz becomes positive due to the coverage of $Ca(OH)^+$ ions on the surface, which provides enough binding sites for the anionic polymer to attach.

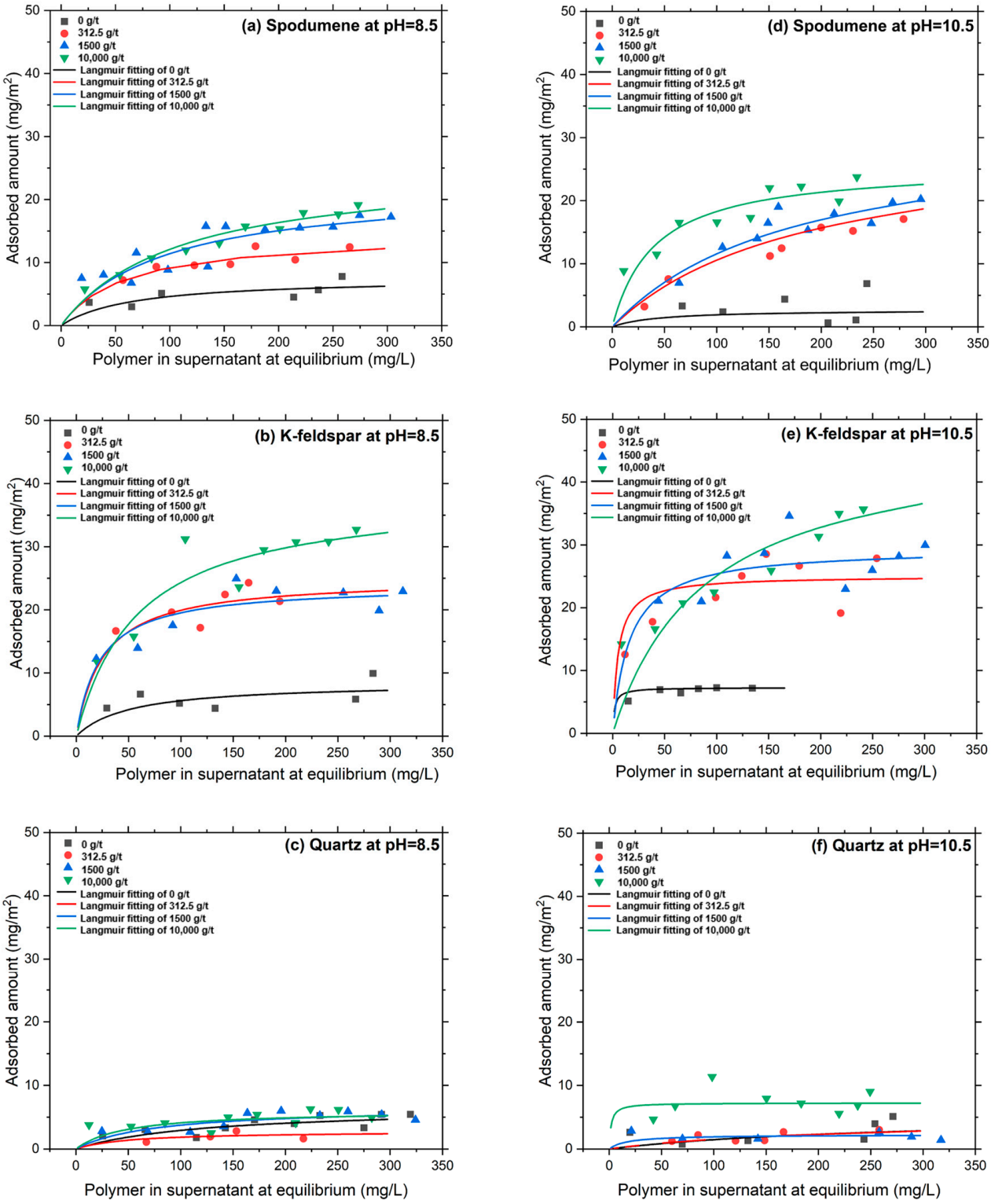


**Figure 3.** Comparative adsorption isotherms of the 58% anionic-charged polymer (A150) on different mineral surfaces at pH 8.5 and 10.5 with Langmuir model fittings: (**a**) spodumene at pH 8.5, (**d**) spodumene at pH 10.5, (**b**) K-feldspar at pH 8.5, (**e**) K-feldspar at pH 10.5, (**c**) quartz at pH 8.5, (**f**) quartz at pH 10.5. The measurements were taken three times, with each repeat containing four to five points. The combined data from all the runs are presented in the Figure. Appendix A.6, Figure A6 includes the data from all the repeats and the predicted Langmuir fittings based on the 95% confidence interval of the chosen conditions, to demonstrate the reproducibility of the measurements. Data shown as mg/m$^2$ verses mg/L. Appendix A.7, Figure A7 expresses the adsorbed amount in units of mg/g. Appendix A.8, Figure A8 shows the adsorbed amounts in units of mmol/m$^2$.

Overall, K-feldspar and spodumene exhibit similar adsorption isotherms, demonstrating that increased calcium concentrations lead to enhanced polymer adsorption on the particles. This is corroborated by the zeta potential measurements (Figure 1), indicating that higher calcium levels result in positive surfaces on spodumene and K-feldspar. Figure 2 shows more calcium adsorbing onto spodumene and K-feldspar, thereby facilitating polymer binding. However, quartz displays a lower amount of polymer adsorption at pH 8.5, which only increases at pH 10.5 with calcium concentrations of 10,000 g/t. The maximum adsorption is 8 mg/m$^2$ for quartz, in contrast to 20 mg/m$^2$ for spodumene and 30 mg/m$^2$ for K-feldspar at 10,000 g/t calcium. The polymer adsorption onto K-feldspar appears slightly increased compared to spodumene at a pH of 8.5 and a calcium concentration of 312.5 g/t, likely due to the less negative surface of K-feldspar, facilitating easier polymer attachment. However, when the calcium concentration reaches 1500 g/t, spodumene exhibits a positive charge, whereas K-feldspar remains negative. The stronger adsorption onto K-feldspar may be attributed to its ability to adsorb more calcium (Figure 2), as evidenced by the zeta potential measurements (Figure 1) showing that the spodumene zeta potential barely increases above 1250 g/t of calcium, whereas K-feldspar can adsorb additional calcium, providing more binding sites for polymers. The caveat on this discussion is that the zeta potential measurements and adsorption measurements were performed at different solids concentrations, so it is not expected that there is a direct correspondence between these different measurements due to differences in the surface area-to-solution volume ratios. Overall, the results suggest it is possible to aggregate spodumene and likely K-feldspar under conditions where quartz will not be aggregated.

### *3.2. Aggregation Behaviour*

#### 3.2.1. Effect of Calcium Activation

Based on the results in the previous sections, the selective aggregation of spodumene from quartz appears to be potentially viable at both pH 8.5 and 10.5. The zeta potential measurements suggest a better performance at pH 8.5, as quartz may be activated at high pHs. The preliminary aggregation experiments at a pH of 10.5 did not result in the improved selective aggregation of spodumene. In addition, most spodumene flotation is typically conducted around pH 8–8.5 to achieve selectivity for spodumene [8,68,69]. Hence, in the remainder of this paper, the results are focused on a pH of 8.5 as a more suitable condition to selectively flocculate fine spodumene.

The in situ images captured by the Blaze probe are shown in Figure 4a for spodumene, (b) for K-feldspar, and (c) for quartz. The control image for each mineral (a1, b1, c1) shows unaggregated primary particles (like stars in the sky). In part 2 of each image, only the polymer has been added, and the spodumene, K-feldspar, and quartz are not significantly aggregated under these conditions. However, as shown in part 3, spodumene and K-feldspar do aggregate when both the polymer and calcium are present. The aggregates of spodumene are more prominent and appear larger than those of K-feldspar. The quartz is not aggregated even in the presence of both the polymer and calcium at the studied concentrations.

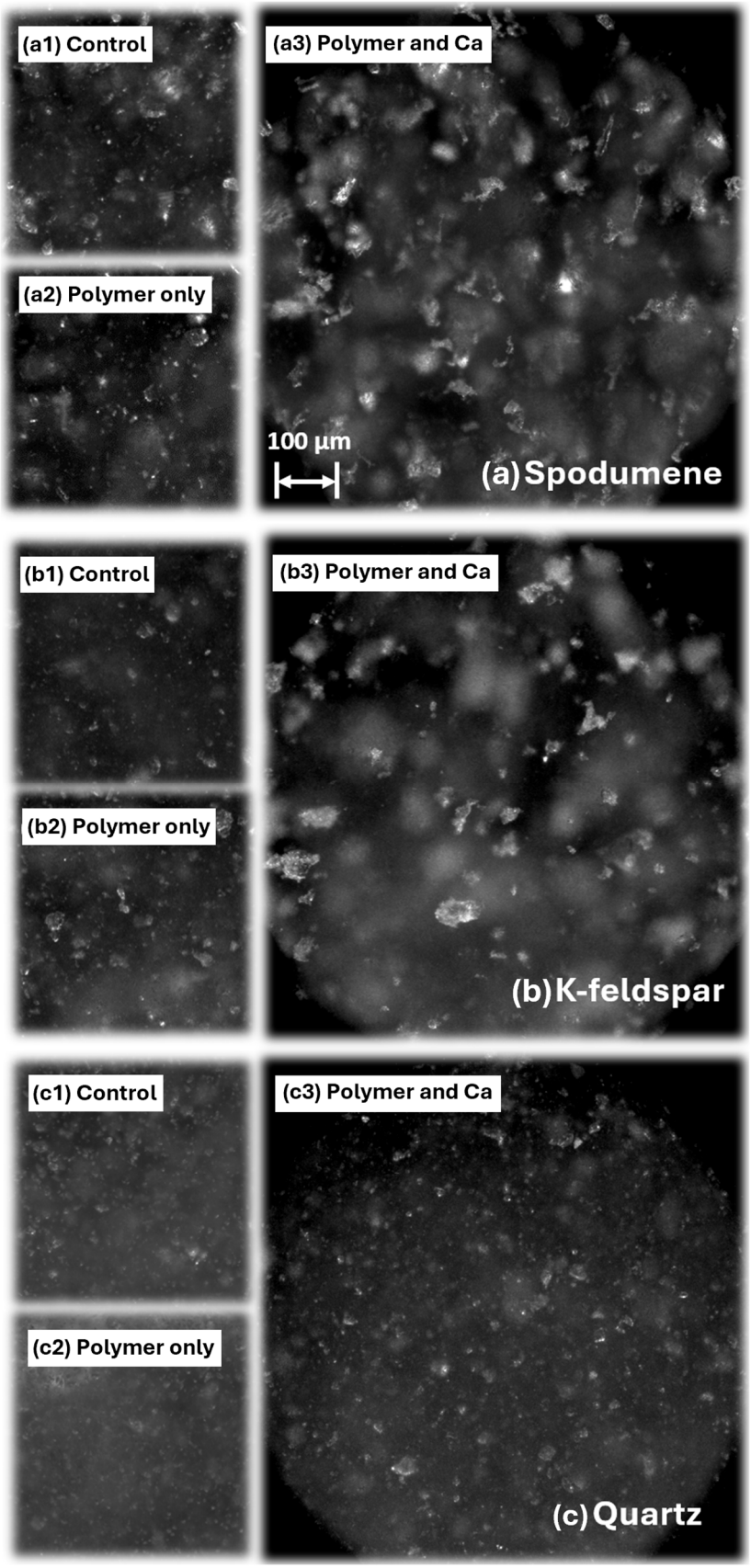


**Figure 4.** In situ probe images depicting various minerals. (**a**) Spodumene, (**b**) K-feldspar, and (**c**) quartz at pH 8.5 under different conditions: (1) without polymer and without calcium ions, (2) with polymer (84 g/t) but without calcium ions, and (3) with both polymer (84 g/t) and calcium ions (625 g/t). All images are presented at the same scale for direct comparison.

### 3.2.2. Effects of Polymer Concentration

The Blaze probe software processes images, such as those shown in Figure 4, to obtain the chord length distributions, as shown in Figure 5. To understand the influence of the polymer dosage at a constant calcium concentration, Figure 5 shows the length- and cube-weighted chord length distributions measured 5 min after the addition of the polymer at pH 8.5 in the presence of 625 g/t of calcium. The polymer employed in this study was of 58% anionic charge (A150).

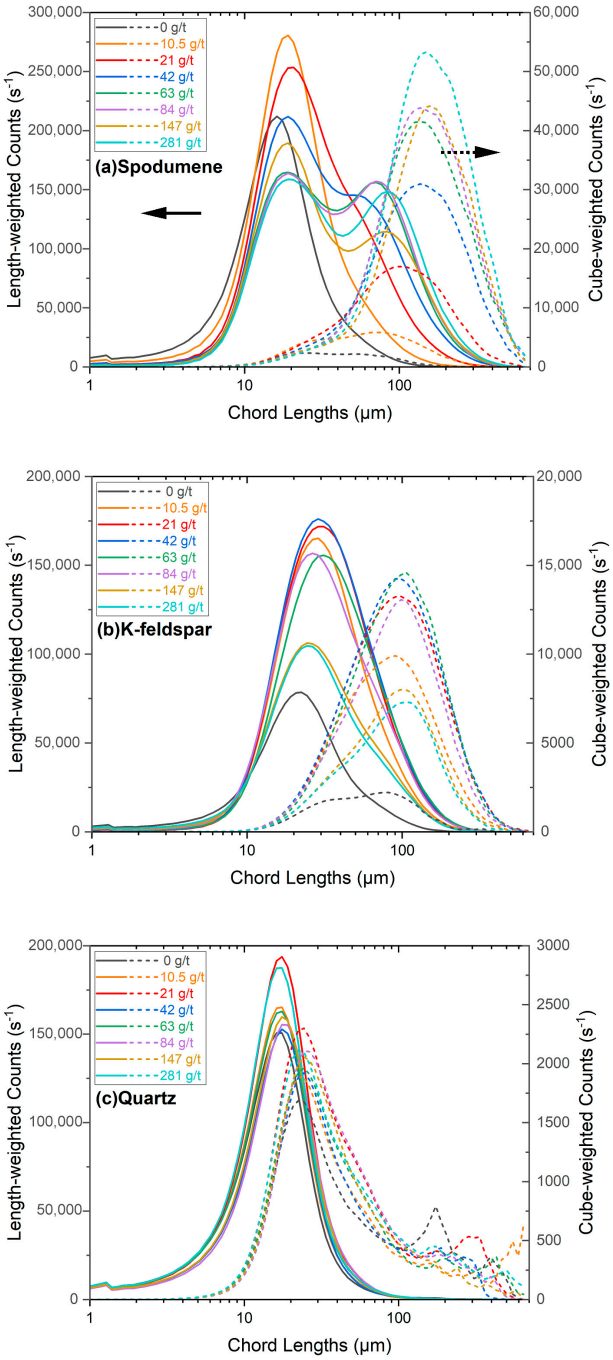


**Figure 5.** Length- and cube-weighted chord lengths measured 5 min after the addition of the polymer at pH 8.5, with a constant calcium concentration of 625 g/t and varying dosages of 58% anionic charge polymer (A150): (**a**) spodumene, (**b**) K-feldspar, (**c**) quartz. Examples of the reproducibility of some conditions is shown in the Appendix A.9. Several conditions were repeated to test the reproducibility, and these are shown in Appendix A.9, Figure A9.

For spodumene, the length-weighted distribution reveals a trend where the peak shifts to larger chord lengths and broadens as the polymer concentration increases from 0 to 21 g/t, indicating the formation of some aggerates. With a further increase in the polymer concentration, the peak at around 15 μm begins to decrease, and the emergence of a second peak around 50 μm indicates the formation of larger aggregates in addition to the primary particles. The aggregates grow and the counts of the primary particles decrease with an increasing concentration above 42 g/t. Further increasing the polymer concentration causes the second peak to shift towards 80 μm. The larger measured chord lengths indicate the formation of larger particle aggregates at higher polymer concentrations. The corresponding cube-weighted distributions (represented by the dotted lines) also shift towards larger sizes as the polymer concentration is increased. The peak (mode) of the aggregate size distributions of the spodumene aggregates with more than 42 g/t of polymer occur at about 130 to 160 μm. The cube-weighted counts at the peak chord length increase from 4000 to 30,000 with the addition of 42 g/t of polymer, and exceed 50,000 counts at the highest dosage of 281 g/t of polymer. This suggests that the amount (volume) of aggregates increases with the polymer dose.

As observed in Figure 5a, the peaks of the cube-weighted counts of spodumene with the addition of 63 g/t to 147 g/t of polymer show no major differences, only increasing dramatically after 281 g/t. This suggests that at around 63 g/t, the polymer concentration is sufficient to aggregate the spodumene. This is why, in a later section, 42 g/t of polymer is used for monitoring the effect of the calcium ions concentration on the aggregation behaviours and selective sedimentation. The purpose of the selective aggregation presented here is to prepare for future flotation experiments, where some adsorption sites on the surface of the spodumene need to be preserved for subsequent collector attachment.

For K-feldspar, the length-weighted distributions show a pronounced peak shift towards larger sizes and slightly narrower peaks with an increase in the peak intensity as the polymer concentration increases from 0 to 42 g/t. Unlike spodumene, it does not show a second peak at a larger length-weighted distribution after the polymer addition. Instead, the peak length-weighted chord appears to increase from 20 μm to 30 μm up to 42 g/t, where the count reaches a maximum of just above 150,000. This may mean that more particles were detected or small aggregates were formed without a significant change in their overall size distribution. A further increase in the polymer dosage leads to a diminishing and broadening of the peaks, along with a lower intensity, and the length-weighted counts at the maximum chord length surprisingly drop from above 150,000 to near 100,000. This suggests a decrease in the number of primary particles, as they were included within the larger aggregates. The cube-weighted distributions confirm the trend of larger aggregates. With an increasing amount of polymer, the peaks shift to the right (larger size). The peak intensity increases from 0 to 63 g/t, peaking at 63 g/t, with a peak chord length (mode) of around 100 to 120 μm. Further polymer addition continues to shift the peak slightly to the right, but the intensity drops with the increasing polymer concentration. Compared to spodumene, the maximum peak counts are lower, suggesting fewer aggregates. In addition, the peak counts decrease with a polymer dose above 84 g/t, with potentially fewer aggregates due to overdosing.

The length-weighted counts of the quartz suspension show no shift towards a larger chord length with an increasing polymer concentration, suggesting no significant aggregation at this concentration of calcium. This is consistent with the results of the polymer adsorption studies in Figure 3, that show less adsorption onto quartz than spodumene and K-feldspar. The cube-weighted counts for quartz indicate little aggregation, as the mode of these distributions remains around 20 to 30 μm. In addition, the cube-weighted peak counts are also low, at around 2000. There was no significant aggregation of quartz. It should

be noted that the small peaks in the quartz cube-weighted distributions at 200 to 400 µm are not due to aggregates. Instead, these peaks are due to artefacts during the visual measurement, where large (200–400 µm) bright flashes, presumably due to reflections off the quartz, were occasionally observed, as reported previously [42]. These visual artefacts were not observed with spodumene and K-feldspar. It can be seen from Figure 4 that no significant quartz aggregation was present.

#### 3.2.3. Effect of Calcium Concentration

Figure 6 shows the length- and cube-weighted chord lengths measured 5 min after the addition of the polymer at pH 8.5 in the presence of 42 g/t of 58% anionic-charged polymer (A150) and various doses of calcium. For spodumene, as the calcium concentration increases from 0 to 5000 g/t, the length-weighted distribution curves (solid lines) shift towards larger chord lengths and a second peak forms, indicating the formation of aggregates. Even at a low calcium concentration of 312.5 g/t, the length-weighted counts of the chord distribution for spodumene show aggregation. However, calcium concentrations above 5000 g/t cause the peaks to shift to the left, indicating the formation of smaller aggregates. Similarly, the cube-weighted distribution (dotted lines) shows a shift towards larger sizes with increasing calcium concentrations, with the mode of the distributions around 120 to 140 µm. The number of counts at the peak (mode) of the cube-weighted distribution is most pronounced at a concentration range of 312.5 to 2500 g/t, suggesting the formation of a larger volume of aggregates within this range. However, this peak drops to lower counts at higher concentrations when the calcium concentration reaches 5000 g/t and above.

The K-feldspar length-weighted distribution curves in Figure 6b demonstrate an increase in the aggregate size with increasing calcium concentrations. Similar to spodumene, the length-weighted distribution curves show a slight increase in the peak chord length with increasing calcium concentrations, up to 5000 g/t. Beyond this point, the peak chord length begins to decrease, which could indicate reduced aggregate formation. The cube-weighted distribution indicates the largest volume of aggregates was formed at 5000 g/t of calcium. The mode of the largest aggregates of K-feldspar was around 100 to 120 µm. The reduction in the volume of the aggregates at higher concentrations reflects reduced aggregation.

In the case of quartz, both the length-weighted and cube-weighted distributions follow a similar trend. The counts increase only slightly with a calcium concentration below 5000 g/t, and the chord-length peak shifts only slightly to the right. The cube-weighted counts increase significantly when the calcium concentration exceeds 5000 g/t, where the calcium starts to facilitate the adsorption of the polymer to form aggregates. However, the size of the aggregates remains relatively small compared to those for spodumene, with a peak located at about 40 µm.

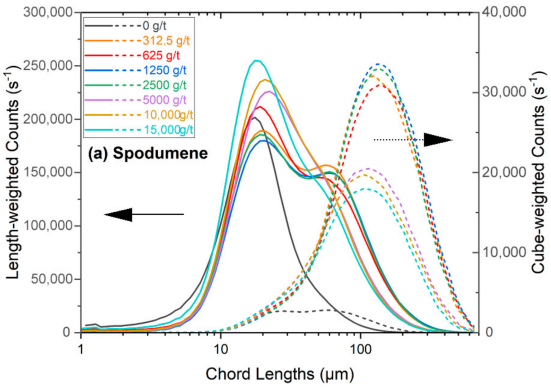


**Figure 6.** *Cont.*

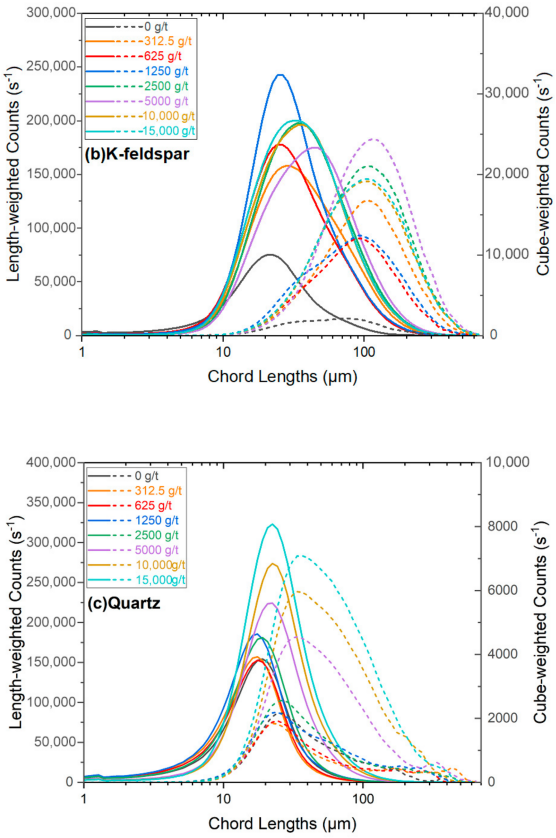


**Figure 6.** Length- and cube-weighted chord lengths measured 5 min after the addition of the polymer at pH 8.5, with a constant polymer concentration and varying dosages of calcium, using 42 g/t of 58% anionic-charged polymer (A150): (**a**) spodumene, (**b**) K-feldspar, (**c**) quartz. Several conditions were repeated to test the reproducibility, and these are shown in Appendix A.9 Figure A9.

### 3.2.4. Effects of Polymer Charge and Molecular Weight

The influence of the polymer charge and molecular weight on the aggregate sizes were also investigated. The details are provided in Figures A11 and A12. The anionic charge on the polymer was varied from <2% (non-ionic polymer) to 58% at pH 8.5 in the presence of 625 g/t of calcium and 42 g/t of the specified polymer. All the polymers induced the aggregation of spodumene, with the peak aggregate size of the cube-weighted chord length distributions at about 130–150 µm. For spodumene, the largest number of aggregates were produced with the 30% charged polymer, which was only slightly larger than the amount produced with the 58% charged polymer. The situation was different for K-feldspar, where the non-ionic polymer produced the largest number of aggregates and the largest peak of the cube-weighted chord length distributions, at about 100–120 µm, whereas the 30% charged polymer was least effective for aggregation. In the case of quartz, only the non-ionic polymer was slightly effective for producing a small number of small aggregates, while the charged polymers were ineffective for flocculating the quartz, primarily due to the charge–charge repulsion between the anionic polymer and the negatively charged quartz surface.

The influence of the polymer molecular weight, as shown in Figure A12 in the Appendix A.13, was investigated at pH 8.5 in the presence of 625 g/t of calcium and 42 g/t of the 30% anionic-charged polymer. The influence of the molecular weight was similar for both spodumene and K-feldspar, where increasing the polymer molecular weight from 6 to about 20 MDa resulted in a larger count of aggregates. The peak in the cube-weighted chord length distribution of the aggregates also slightly increased with the

polymer molecular weight. The molecular weight of the polymer had little influence on the quartz, as no significant aggregation was observed with the charged anionic polymers.

### *3.3. Mapping of Aggregation Behaviour*

#### 3.3.1. Aggregate Size

Aggregate size measurements were conducted over a range of calcium concentrations, from 0 to 15,000 g/t of mineral solid particles, and a range of polymer (58% anionic charge) concentrations, from 0 to 280 g/t. The median cube-weighted chord length was determined for each condition for spodumene, K-feldspar, and quartz. The cube-weighted chord length distribution is utilised here to provide values that are more comparable to the volume-weighted distribution used in other sizing techniques. The results are presented in the form of a heatmap in Figure 7.

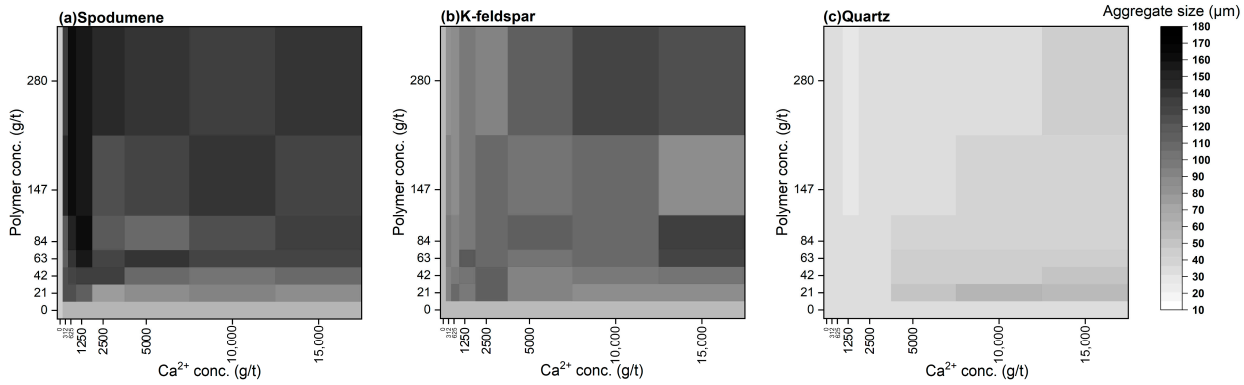


**Figure 7.** Impact of calcium concentration and 58% anionic-charged polymer (A150) dosage on the median cube-weighted aggregate size during the aggregation of spodumene, K-feldspar, and quartz at pH 8.5. White corresponds to a particle size of 10 µm and black corresponds to an aggregate size of 180 µm. For the aggregate size measurements, two or three measurements were taken for some of the conditions, and the average is shown here. The reproducibility and consistency of some of the conditions are demonstrated in Appendix A.9, Figure A9.

For spodumene, the heatmap appears mostly dark, indicating that under most of the combinations of calcium and polymer, large aggregates were produced. This suggests that even the lowest investigated amount of calcium (312.5 g/t) and polymer (21 g/t) might be sufficient for some aggregation, with a measured median cube-weighted chord length of about 80 µm. Without calcium, the polymer itself did not appear to produce spodumene aggregates, which is consistent with Figure 4 and the turbidity study that will be presented in the next section. This observation aligns with the zeta potential measurements (Figure 1) showing that, in the absence of calcium, the spodumene surfaces remain negatively charged, making it difficult for the anionic polymer to adsorb. Calcium facilitates adsorption, perhaps, by providing a bridge between the carboxylate groups of the polymer and the spodumene surface. The largest aggregates were produced when the calcium was lower than 2500 g/t but the polymer was more than 84 g/t, resulting in an aggregate size >150 µm. This was expected, as an increased number of polymer molecules enhances the rate of collisions, which in turn heightens the chances of the polymer being in an active state, ultimately leading to the formation of larger aggregates. The increased concentration of polymers might also discourage relaxation onto the surface of the minerals due to steric repulsion, aiding in flocculation activity. This might also explain the slight decrease in the size of the measured aggregates following an increase in the calcium dosage above 2500 g/t, as the polymer may attach onto an increased number of sites on the same particle, rather than on multiple particles.

In the case of K-feldspar, the heatmap shows some variability in the shade, with a tendency for darker shades at higher concentrations of both the polymer and calcium, indicative of larger aggregate sizes near 100 μm. This could imply that K-feldspar particles tend to form larger aggregates as the calcium ion and polymer concentrations increase. This aligns with the findings from the turbidity measurements, presented in the next section, and suggests that, similarly to spodumene, a higher polymer concentration produces larger aggregates. However, unlike spodumene, the larger aggregates in the K-feldspar are associated with higher calcium concentrations. This suggests that for K-feldspar to aggregate, more calcium is required to bind the polymer to the surface. In the region where spodumene produced the largest aggregates (625 g/t to 2500 g/t calcium and >42 g/t polymer), the K-feldspar aggregates were typically smaller (about 50 to 80 μm) than the spodumene aggregates. The reason K-feldspar requires more calcium to form larger aggregates compared to spodumene could be that higher calcium concentrations are required to reverse the zeta potential to a positive charge (see Figure 1b). The careful control of the calcium concentration may be useful for separating spodumene from K-feldspar, although it may be difficult to aggregate only spodumene without forming at least small aggregates of K-feldspar.

For quartz, the heatmap shows there was very little aggregation. Some small aggregates formed when the calcium concentration was more than 5000 g/t, particularly at lower polymer concentrations. Even a high polymer concentration was not enough to form aggregates when the calcium was below 5000 g/t. This can be explained by the low adsorption of calcium onto quartz (see Figure 2). A high concentration of calcium is required to facilitate the attachment of the polymer onto the surface of quartz for aggregation. Compared to spodumene and K-feldspar, in most cases, quartz does not aggregate unless the calcium concentration is high. This could be because the zeta potential of quartz has a mostly negative charge. Even though calcium is present on the surface, the highly negative charge may discourage the attachment of the anionic polymer. However, when the concentration is high enough, regardless of the overall negative charge, the polymer will nevertheless bind to the calcium on the quartz surface.

There is a region where the calcium concentration is between about 312.5 g/t and 2500 g/t, and the polymer concentration is greater than about 42 g/t, where spodumene aggregates with a size of about 150 μm while quartz does not aggregate, which represents a possible avenue for spodumene to be selectively aggregated from quartz. K-feldspar will also form aggregates, albeit a bit smaller (100 μm) than spodumene. Under these conditions, it may be difficult to selectively aggregate spodumene from K-feldspar.

#### 3.3.2. Turbidity

The turbidity of the supernatants of the suspensions following 5 min of mixing and 2 min of settling was measured over a range of calcium concentrations, from 0 to 15,000 g/t of solids, and a range of polymer concentrations (58% anionic charge), from 0 to 280 g/t. High turbidity indicates poor aggregation, as the majority of particles remain suspended in the supernatant, while low turbidity indicates good aggregation and the rapid sedimentation of the aggregates. Figure 8 shows the heatmaps for the turbidity of the spodumene, K-feldspar, and quartz supernatants. The results are presented in NTU (Nephelometric Turbidity Units) as a function of the concentrations of calcium ions and polymer.

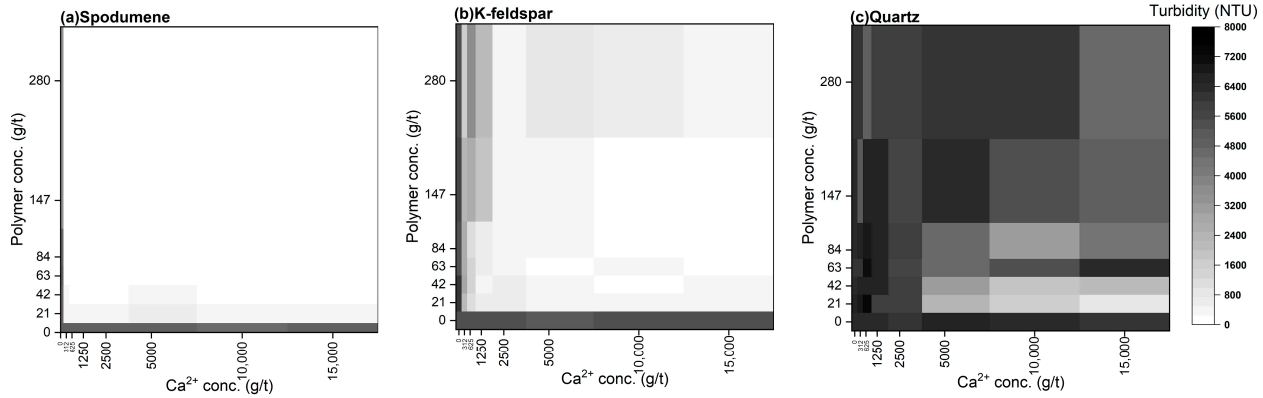


**Figure 8.** Comparative turbidity levels for the selective aggregation of spodumene, K-feldspar, and quartz, with varying calcium ion concentrations and 58% charged anionic polymer (A150) dosages at pH 8.5. White indicates 0 NTU (clear liquid), while black corresponds to 8000 NTU (turbid suspension). For the turbidity measurements, two or three measurements were taken for some of the conditions, and the average is shown here. The numerical values for the turbidity readings, including the 95% confidence interval for the repeated measurements, are included in Appendix A.14, Table A2.

For spodumene, no aggregation was observed if either calcium or the polymer was absent, as indicated by the high turbidity values. The heatmap demonstrates low turbidity, with a relatively uniform distribution of white across the ranges of calcium ions and polymer concentrations investigated. This suggests that even a small amount of calcium (312.5 g/t) and polymer (20 g/t) might be sufficient for the aggregation and settling of spodumene suspensions. The turbidity results are consistent with the aggregate size results presented in Figures 5–7.

The K-feldspar heatmap displays behaviour similar to that of spodumene. The presence of calcium ions at various concentrations without the polymer, as well as varying concentrations of the polymer without calcium, did not lead to aggregation, as evidenced by the high turbidity levels. At low calcium concentrations (<1250 g/t), there was a slight increase in turbidity with increasing polymer concentrations, with the darker shades indicating higher turbidity levels. Surprisingly, more polymer resulted in darker shades, signifying less aggregation, although this trend was not as apparent with calcium concentrations over 5000 g/t. This indicates that the K-feldspar supernatants became less transparent and exhibited less aggregation as the polymer concentration increased, possibly due to a less effective flocculation process resulting in smaller aggregates and some unaggregated particles. However, most of the heatmap area, which includes both polymer and calcium ions, shows a relatively uniform light colour, indicating that aggregation occurred in most scenarios.

Quartz, on the other hand, displayed little to no aggregation in most cases, with the darkest intensities indicating the highest turbidity at low calcium ion concentrations, regardless of the polymer concentrations. When the calcium concentration exceeded 5000 g/t, the supernatant began to clear at lower polymer dosages. The higher the calcium concentration, the clearer the supernatant became, indicating more successful aggregation, consistent with the aggregate size measurements in Figure 6 and with the literature [56] suggesting that calcium can activate quartz to adsorb carboxylate functional reagents at higher calcium concentrations.

### *3.4. Sedimentation Studies*

As demonstrated in the previous sections, K-feldspar and spodumene exhibit relatively similar adsorption and aggregation behaviours under the same conditions. Although K-feldspar appears to form fewer and smaller aggregates than spodumene, K-feldspar can still be activated by calcium ions, and the A150 polymer can adsorb to K-feldspar. To

simplify the sedimentation tests, only spodumene and quartz were investigated, as quartz is the predominant gangue mineral present in spodumene-containing lithium ore [20].

Mixed mineral suspensions containing a 3:7 weight ratio of spodumene to quartz were treated with 42 g/t of 58% charged anionic polymer (A150) in combination with 625 g/t of calcium, where g/t refers to the grams of calcium or polymer per total mass of the sample (the mixture of quartz and spodumene). The mixed suspensions were then allowed to settle in an attempt to separate the minerals. The polymer specifically targeted the spodumene in an attempt to separate it from the quartz. The goal was to maximise the recovery of spodumene in the sediment and the rejection of the quartz in the supernatant, starting from a feed grade of 30% spodumene.

As shown in Figure 9a, without the polymer, 68% of the spodumene was recovered in the sediment, while 47% of the quartz was also reported to be in the sediment. After the polymer addition (10 wt% suspension, 5 min mixing, 2 min settling), the recovery of spodumene in the sediment increased dramatically to 98%, indicating efficient aggregation and settling, whereas the quartz recovery also increased, but to a lesser extent (81%). The increased quartz recovery in the sediment is likely due to entrapment or potentially surface sliming effects since, as shown in Sections 3.2 and 3.3, quartz is not aggregated under these conditions. When the mineral mixture suspension concentration was reduced to 5 wt%, the recovery of spodumene in the sediment slightly decreased to 94%, and the quartz recovery decreased more significantly to 59%, suggesting that a lower solids concentration in mixed mineral suspensions is more effective for selective spodumene aggregation, potentially due to reduced entrapment and/or sliming. With a reduced mixing time (2 min) but maintaining a 10 wt% suspension, the highest sediment recovery of spodumene was achieved, at 99%, while the quartz sediment recovery remained high at 80%, indicating that shorter mixing produced only a slight improvement compared to a 5 min mixing time. Conversely, a shorter settling time (1 min) with the same polymer concentration and mixing time reduced the sediment recovery for both spodumene (70%) and quartz (37%), indicating an insufficient settling time for complete separation. Thus, the polymer addition, along with the optimised mixing and settling times, enhanced the aggregation and sedimentation of spodumene, although quartz was also recovered, likely by entrapment.

Figure 9b illustrates the grades of spodumene and quartz in the sediment and supernatant under the various conditions. Without the polymer (10 wt% suspension, 5 min mixing, 2 min settling), the spodumene had a sediment grade of 44% (the recovery was 68%). With the addition of the polymer (10 wt% suspension, 5 min mixing, 2 min settling), the sediment grade of the spodumene decreased to 28%, and the recovery was 98%, indicating effective separation but with significant quartz entrapment. Reducing the suspension concentration to 5 wt% (5 min mixing, 2 min settling) slightly increased the spodumene grade to 31%, suggesting a limited improvement in the separation efficiency, since the grade was close to the feed grade. Decreasing the mixing time to 2 min (10 wt% suspension, 2 min settling) resulted in a slight reduction in the spodumene grade to 27%. Conversely, reducing the settling time to 1 min (10 wt% suspension, 5 min mixing) increased the spodumene grade to 33%. After the addition of the polymer, the grade of the spodumene dropped to around the feed grade, which shows that sedimentation is not a good way to separate aggregates. Potentially, flocculation followed by froth flotation may be a more effective way to reach both a high grade and recovery of aggregated spodumene form quartz.

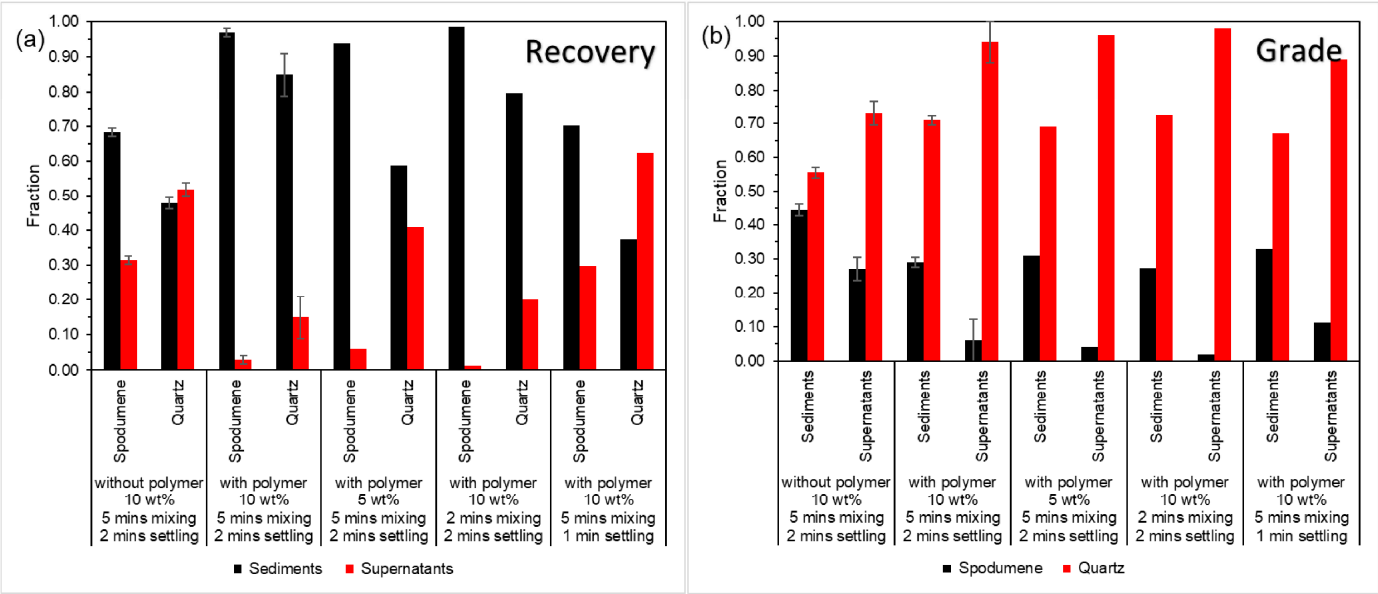


**Figure 9.** Comparison of spodumene and quartz recovery (**a**) and grade (**b**) in sediments and supernatants under various conditions, with different concentrations of suspension (10 wt% and 5 wt%), mixing times (5 min and 2 min), and settling times (2 min and 1 min). All tests used 625 g/t of calcium. Certain conditions were repeated, and these are shown with error bars that represent 95% confidence interval. For these tests, values represent averages of repeat measurements.

### *3.5. Future Work*

The selective aggregation of spodumene from quartz has been successfully demonstrated under optimised conditions. It has also been observed that K-feldspar readily aggregates under similar conditions (in the presence of calcium ions and anionic polymers) as spodumene. It is well recognised in flotation studies that K-feldspar is difficult to separate from spodumene, due to their similar surface properties and flotation behaviours [60,70,71]. However, the aggregation behaviour of K-feldspar under calcium activation and anionic polymer addition has not been previously reported as an aggregation-based separation strategy. This newly identified aggregation behaviour adds additional complexity to the achievement of selective beneficiation. The purpose of studying the selective aggregation of fine spodumene was to improve separation, although the sedimentation results showed the limited separation of spodumene and quartz, and the selective aggregation of spodumene and K-feldspar could not be achieved. Flotation remains available as a subsequent step to further resolve these challenges. Future work will focus on developing improved selective aggregation and flotation strategies to enhance the separation of spodumene from both quartz and K-feldspar. Several opportunities exist, including reagent modifications, surface pretreatments, and/or depressants [25,60,61,68,70,72–85].

## 4. Conclusions

A summary of the key findings are as follows:

- The zeta potential and the adsorption measurements confirmed that Ca(II) reduces the negative surface charge of spodumene, K-feldspar, and quartz. A charge reversal occurred at approximately 10,000 g/t of Ca(II) for spodumene and 15,000 g/t for K-feldspar. The adsorption studies showed that Ca(II) preferentially adsorbs onto K-feldspar, followed by spodumene and quartz, enabling polymer attachment.
- The aggregation tests demonstrated that both spodumene and K-feldspar can be aggregated using Ca(II) and anionic polyacrylamide (PAM). Increasing the polymer dosage led to larger aggregates (100–150 μm), and a polymer concentration as low as

63–84 g/t was sufficient to induce aggregation. Aggregation was enhanced with Ca(II) dosages of up to 5000 g/t, but higher concentrations reduced the efficiency.

- A higher polymer molecular weight and higher charge density result in larger aggregates.
- Quartz showed limited aggregation under most conditions due to electrostatic repulsion between the anionic polymer and the negatively charged surface. Small aggregates were observed at high Ca(II) and polymer dosages.
- The selective aggregation of spodumene at 625 g/t of Ca(II) and 63–84 g/t of A150 (58% anionic charge) at pH 8.5 successfully avoided quartz aggregation in the single-mineral tests. The largest spodumene aggregates were formed at 2500 g/t of Ca(II) and 84 g/t of polymer.
- The sedimentation tests using mixed spodumene–quartz systems, however, showed limited separation due to the physical entrapment of quartz in the spodumene aggregates.

The results presented here demonstrate, for the first time, that polyacrylamide flocculants can be used to selectively aggregate spodumene from quartz. Ca(II) is required to facilitate the adsorption of the polymer onto the spodumene surface. The value of this research is that it provides an approach to improve the recovery of fine spodumene normally lost to tailings. By increasing the recovery of fine spodumene, the overall recovery could increase from 60 to 70% up to perhaps 85 to 90% recovery. There are some limitations of this work. The separation of spodumene from quartz by sedimentation was not effective. The entrapment of quartz in the aggregates reduced the grade of the recovered spodumene. Also, the selective aggregation of spodumene from K-feldspar has not yet been achieved. This suggests that it will be difficult to separate spodumene from K-feldspar. Future work should focus on understanding the factors that influence the entrapment of gangue in aggregates in order to avoid gangue in spodumene aggregates. Selective depressants need to be identified to prevent anionic polyacrylamides from aggregating K-feldspar. Finally, integrated aggregation–flotation strategies that explore reagent design, surface modification, and selective depressants should be investigated to improve the separation efficiency compared to sedimentation. These findings will contribute to the more effective and economically viable beneficiation of lithium ores.

**Author Contributions:** D.L.: Investigation, Conceptualisation, Formal Analysis, Data Curation, Methodology, Writing—original draft, and Writing—review and editing. W.S.N.: Investigation, Formal Analysis, Methodology, and Writing—review and editing. G.V.F.: Formal Analysis, Conceptualisation, Methodology, Project Administration, Resources, Supervision, Funding Acquisition, and Writing—review and editing. All authors have read and agreed to the published version of the manuscript.

**Funding:** This work was supported by the Future Battery Industries Cooperative Research Centre and the Australian Research Council for the ARC Centre of Excellence for Enabling Eco-Efficient Beneficiation of Minerals [grant number CE200100009].

**Data Availability Statement:** The original contributions presented in this study are included in the article and Appendix A. Further inquiries can be directed to the corresponding author.

**Acknowledgments:** Thanks to Syensqo and SNF for supplying the polymeric flocculants. The authors acknowledge the funding support from the Future Battery Industries Cooperative Research Centre. The authors acknowledge the funding support from the Australian Research Council for the ARC Centre of Excellence for Enabling Eco-Efficient Beneficiation of Minerals, grant number CE200100009. This work was performed in part at the Materials Characterisation and Fabrication Platform (MCFP) at the University of Melbourne and the Victorian Node of the Australian National Fabrication Facility (ANFF). Thanks also to Raveen Wijesuriya, Raul Cavalida, Wen (April) Li, Jackquline Eardley, and Regina de Medeiros for training and assistance at various stages of this work.

**Conflicts of Interest:** The authors declare that they have no competing interests, and there has been no significant financial support for this work that could have influenced its outcome.

# Appendix A.

## *Appendix A.1. XRD Characterisation*

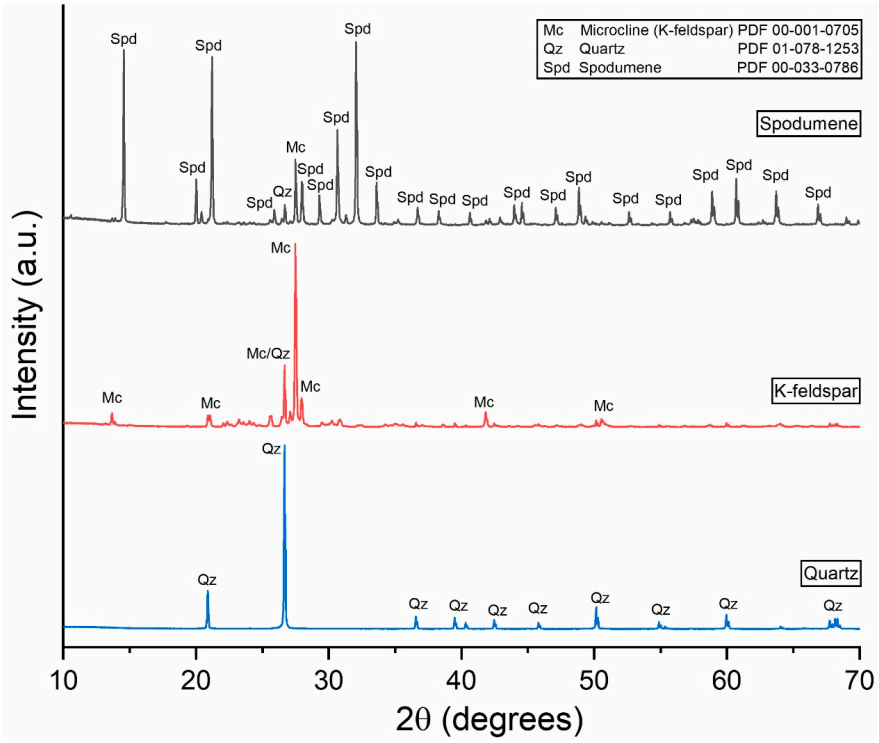


**Figure A1.** XRD patterns of spodumene, K-feldspar, and quartz samples used in this study.

## *Appendix A.2. ICP-OES Characterisation*

**Table A1.** ICP-OES results confirming the elemental composition, including $Al_2O_3$, CaO, $Fe_2O_3$, $K_2O$, Li, and $SiO_2$ (wt%), of the spodumene, K-feldspar, and quartz samples.

| | $Al_2O_3$ (%) | CaO (%) | $Fe_2O_3$ (%) | $K_2O$ (%) | Li (%) | $SiO_2$ (%) |
|---|---|---|---|---|---|---|
| Spodumene | 27.2 | 0.17 | 0.34 | 0.28 | 3.54 | 64.0 |
| K-feldspar | 16.5 | 0.24 | 0.16 | 11.0 | 0.00 | 69.3 |
| Quartz | 0.23 | 0.07 | 0.03 | 0.06 | 0.003 | >99 |

## *Appendix A.3. Particle Size Distributions and Scanning Electron Microscopy (SEM) Images of the Feed Materials*

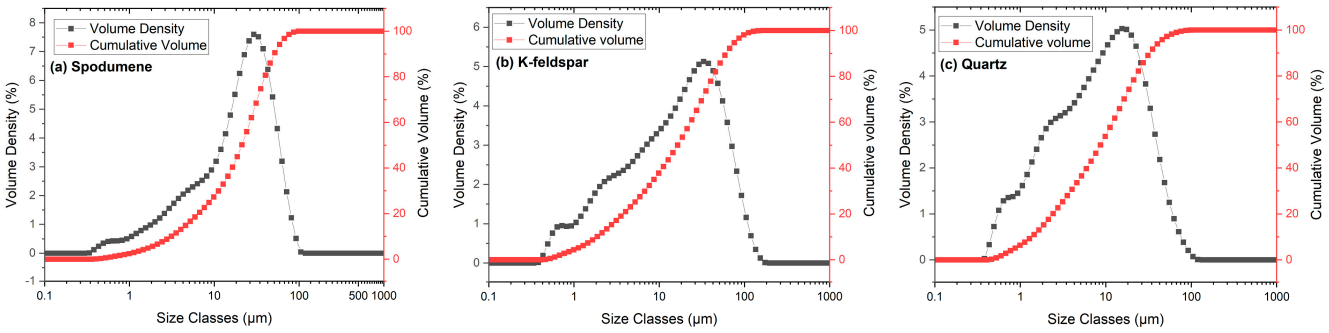


**Figure A2.** Primary particle sizes of the as-received (**a**) spodumene, (**b**) K-feldspar, and (**c**) quartz.

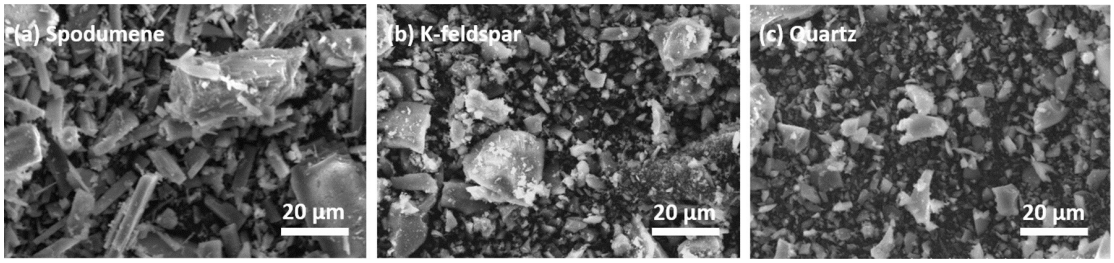


**Figure A3.** SEM images of (**a**) spodumene, (**b**) K-feldspar, and (**c**) quartz viewed at 1200× magnification.

*Appendix A.4. Zeta Potential: Repeat Measurements*

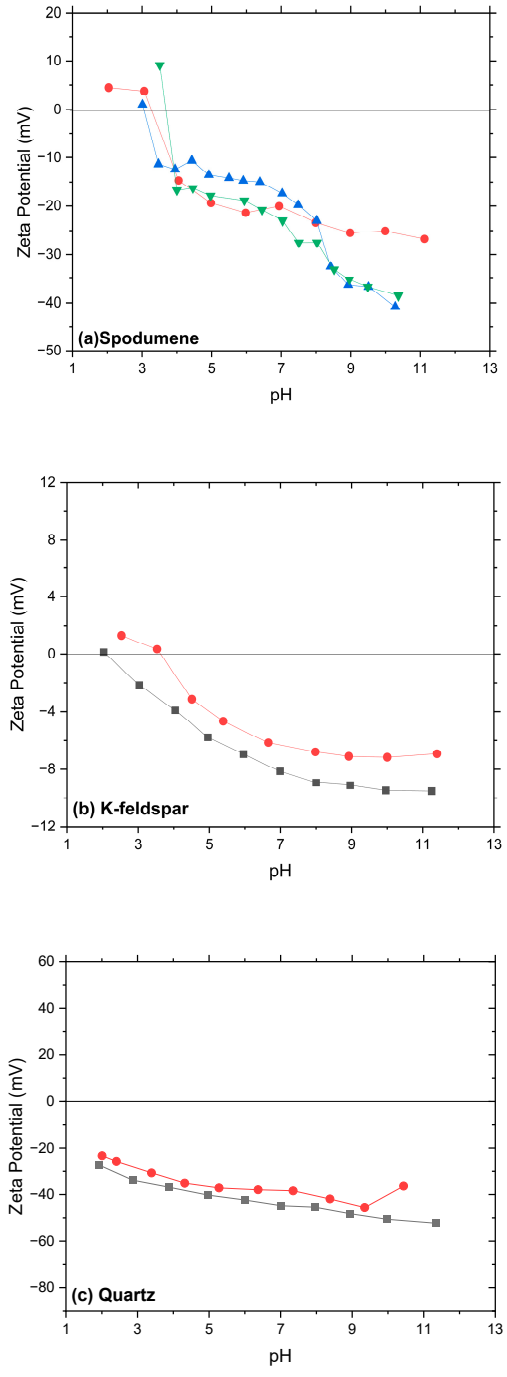


**Figure A4.** Repeat measurements of the zeta potentials of (**a**) spodumene, (**b**) K-feldspar, and (**c**) quartz in the absence of calcium.

*Appendix A.5. Ca(II) Adsorption Isotherms: Repeat Measurements*

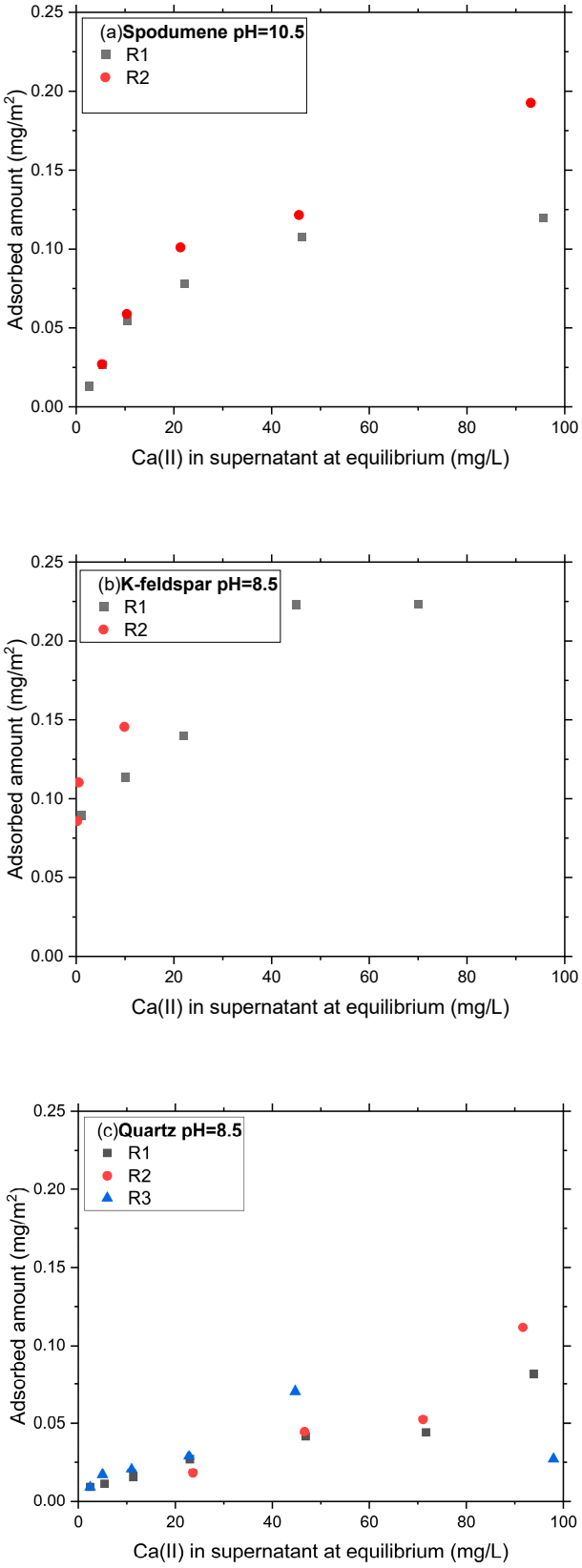


**Figure A5.** Repeat of selected calcium adsorption isotherms to show reproducibility.

*Appendix A.6. Polymer Adsorption Isotherms: Repeat Measurements*

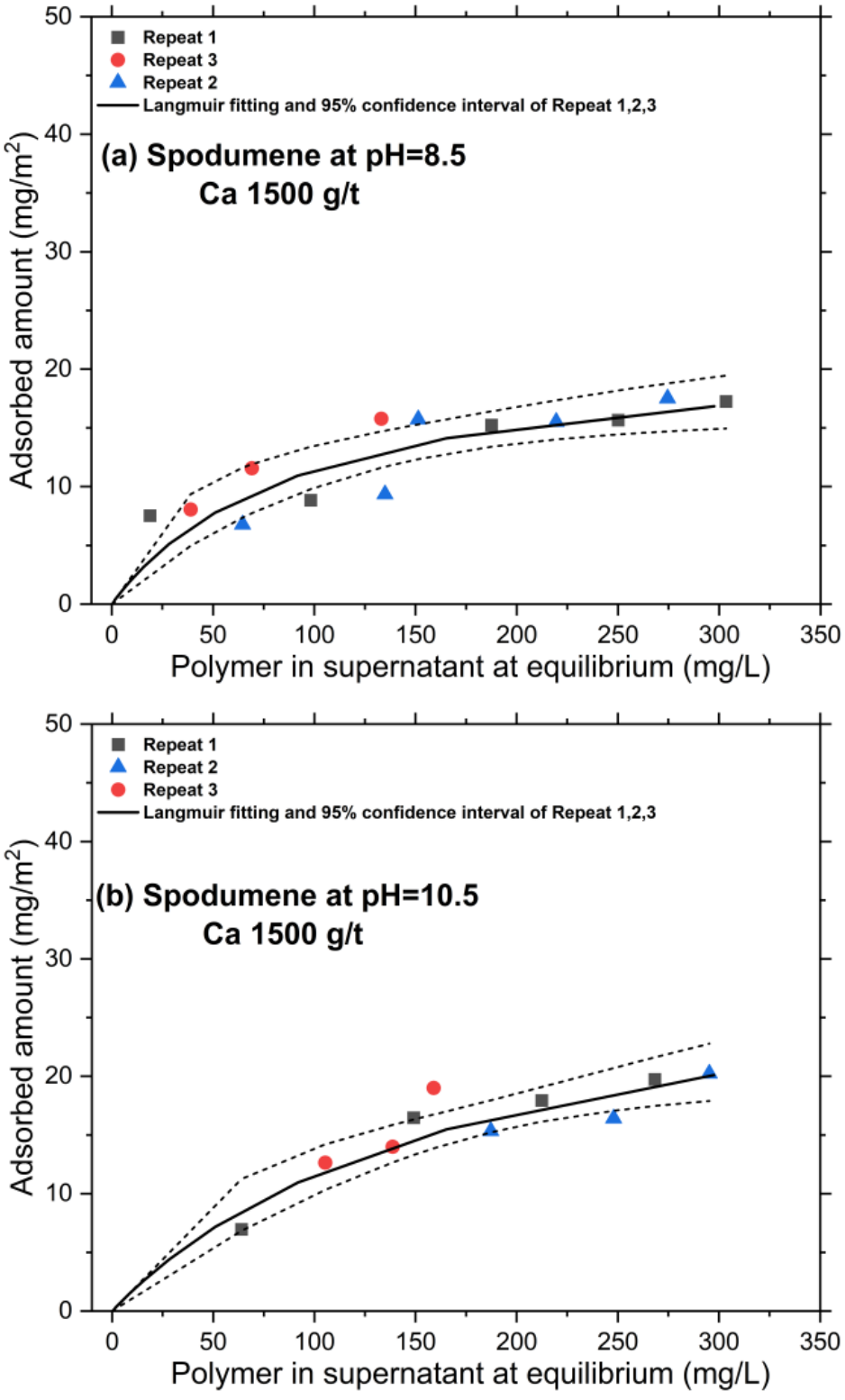


**Figure A6.** The 95% confidence interval of the predicted Langmuir fitting of A150 on spodumene at (**a**) pH 8.5 and (**b**) pH 10.5, with 15,000 g/t of Ca(II), presented as dotted lines. Different colours of the symbols indicate data from three different measurements.

*Appendix A.7. Polymer Adsorption Isotherms*

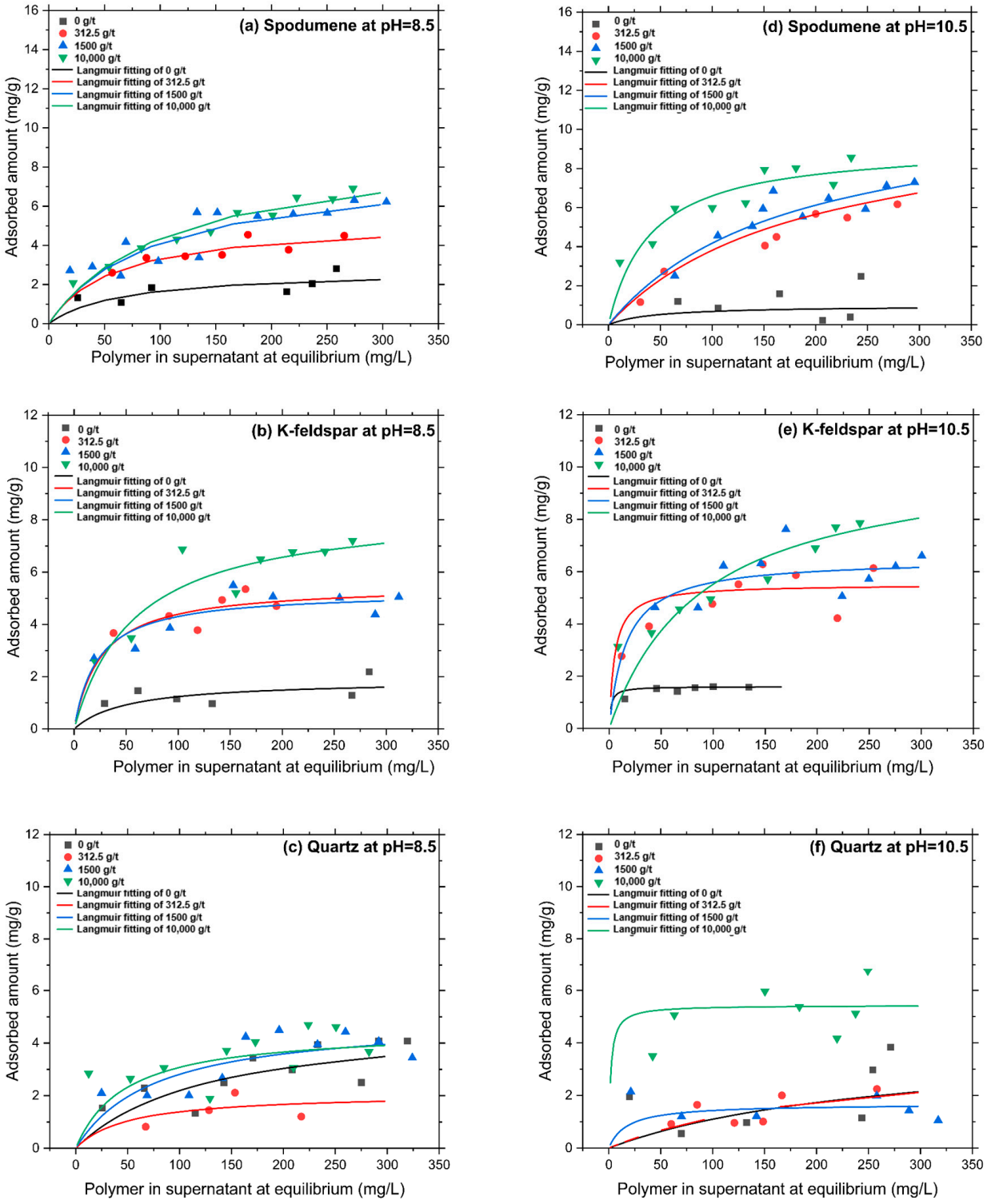


**Figure A7.** Comparative adsorption isotherms of the 58% anionic-charged polymer (A150) on different mineral surfaces at pH 8.5 and 10.5 with Langmuir model fittings: (**a**) spodumene at pH 8.5, (**b**) K-feldspar at pH 8.5, (**c**) quartz at pH 8.5, (**d**) spodumene at pH 10.5, (**e**) K-feldspar at pH 10.5, (**f**) quartz at pH 10.5. Data shown as mg/g verses mg/L.

*Appendix A.8. Polymer Adsorption Isotherms*

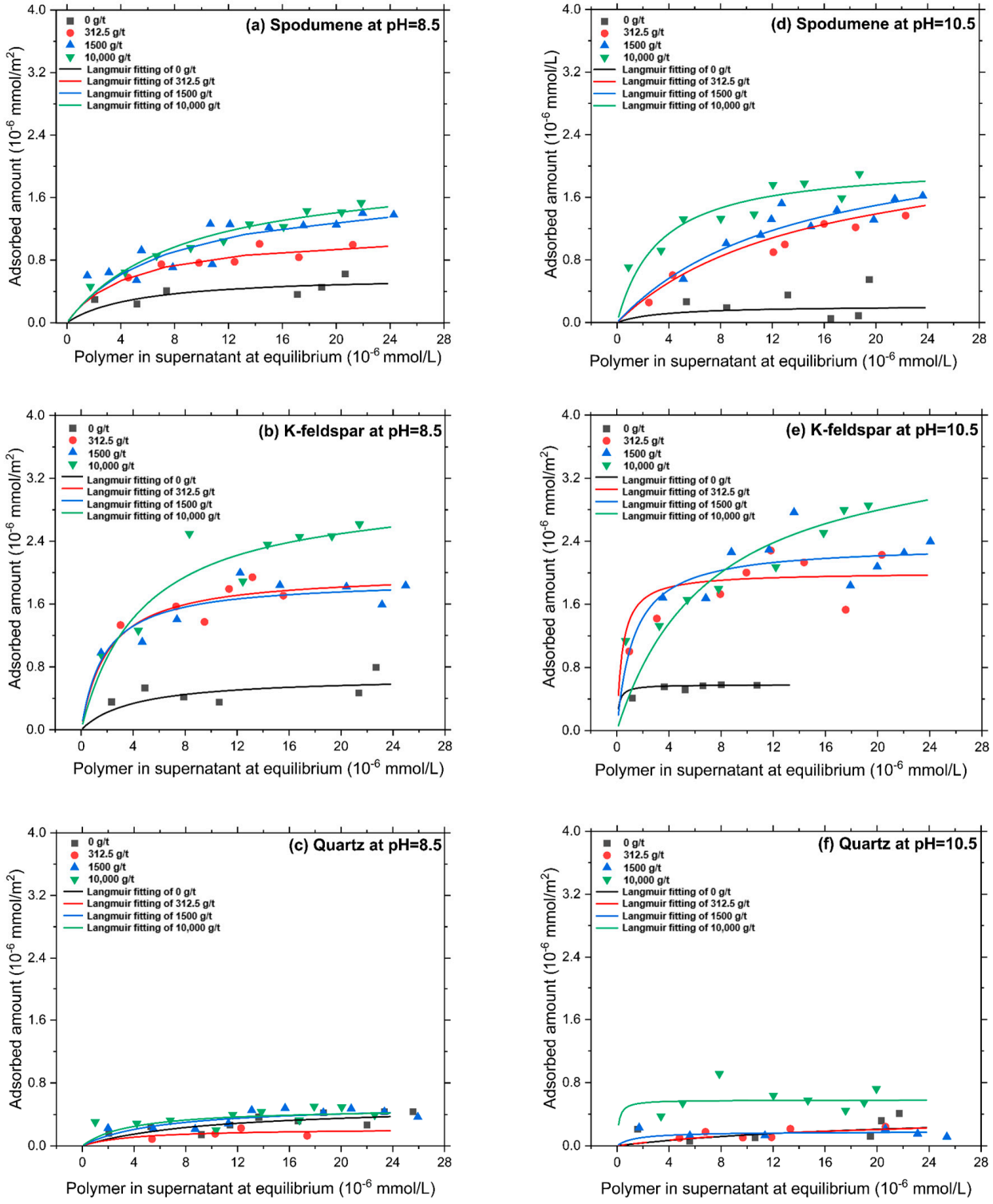


**Figure A8.** Comparative adsorption isotherms of the 58% anionic-charged polymer (A150) on different mineral surfaces at pH 8.5 and 10.5 with Langmuir model fittings: (**a**) spodumene at pH 8.5, (**d**) spodumene at pH 10.5, (**b**) K-feldspar at pH 8.5, (**e**) K-feldspar at pH 10.5, (**c**) quartz at pH 8.5, (**f**) quartz at pH 10.5. Data shown as mmol/$m^2$ verses mmol/L.

*Appendix A.9. Chord Length Distributions: Repeat Measurements*

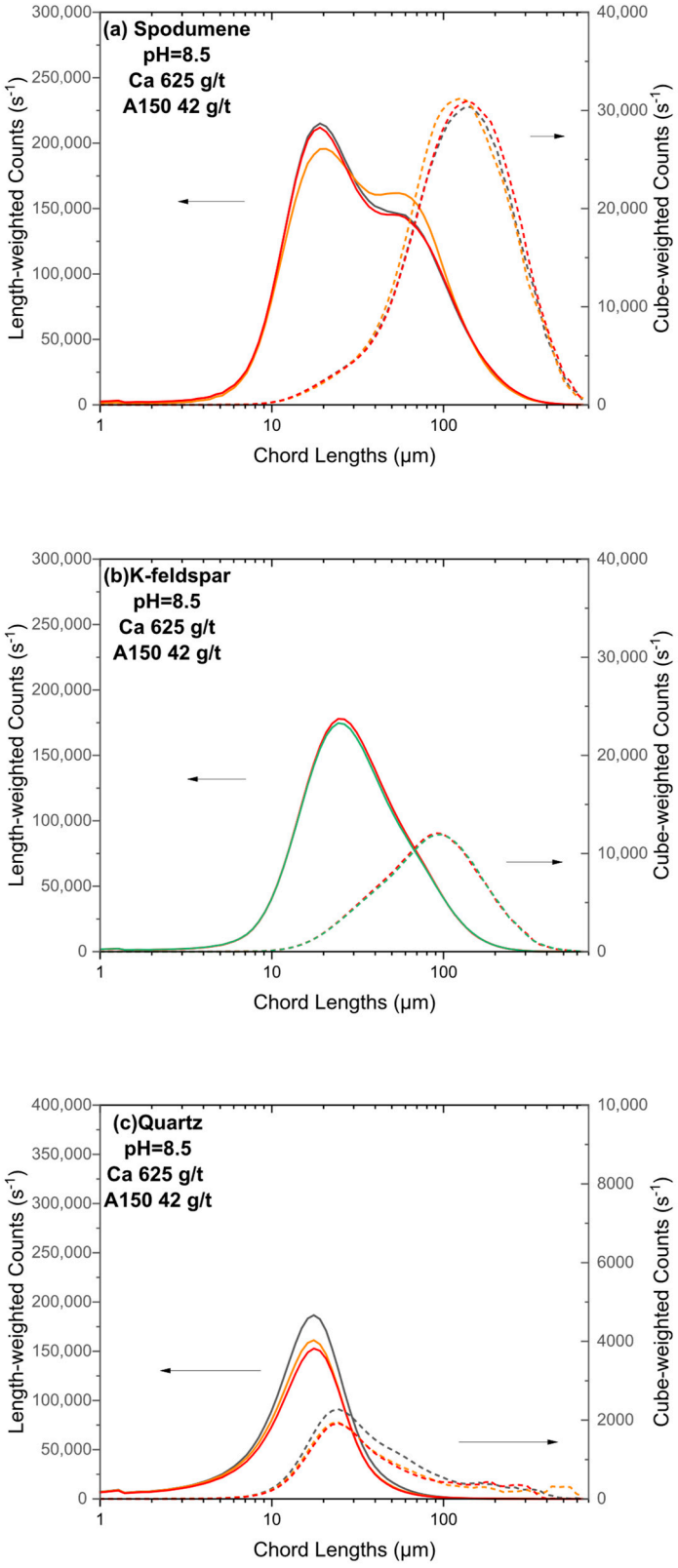


**Figure A9.** *Cont.*

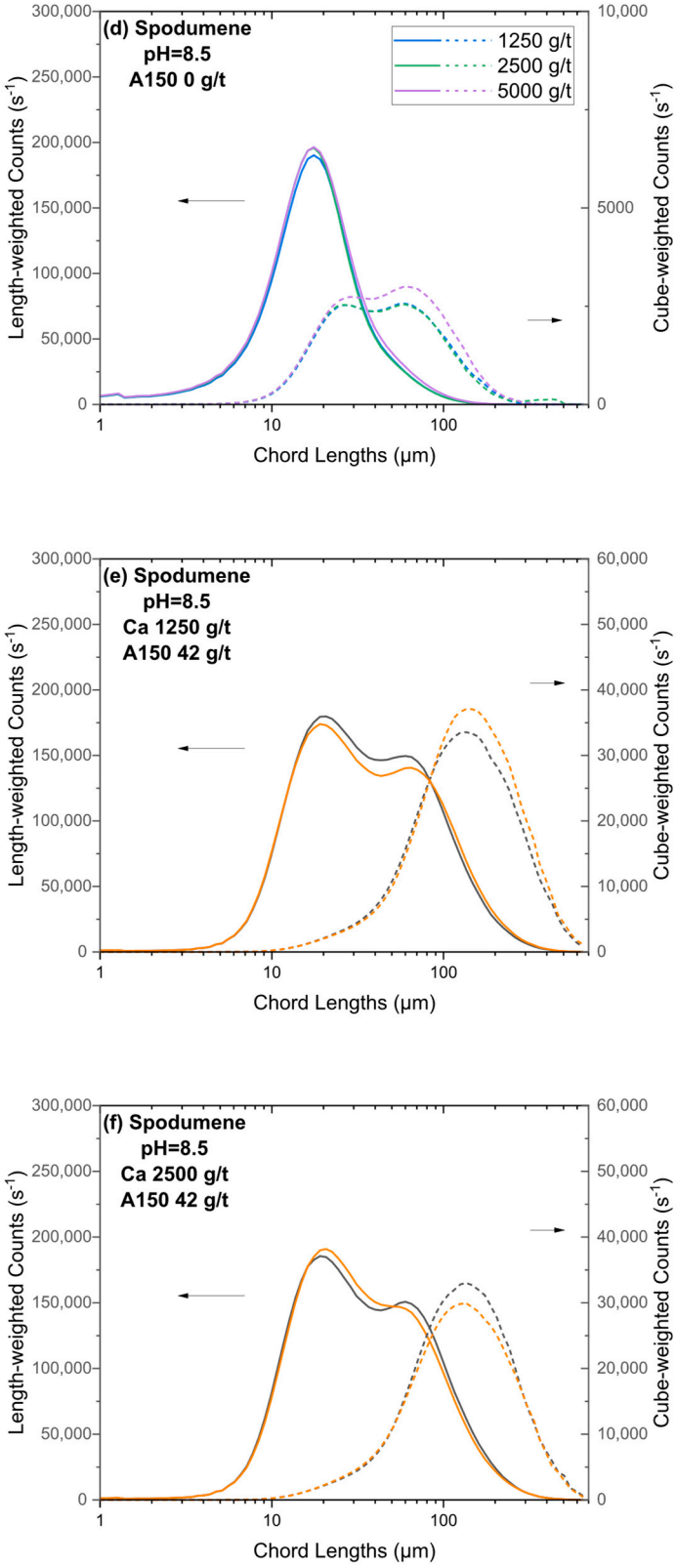


**Figure A9.** Repeats of selected conditions to demonstrate the consistency of the probe measurements under different conditions. The different colours represent measurements from repeat runs under the same conditions, aside from (**d**), where the different colours depict measurements at varying calcium concentrations.

*Appendix A.10. Calibration Curve for Assaying Spodumene*

To establish a calibration curve for determining the spodumene percentage in the spodumene-quartz mixtures, a series of samples were prepared with varying ratios of spodumene to quartz. The mixtures varied in spodumene content from 0% to 100% by weight, specifically at ratios of 0% spodumene to 100% quartz, 20% spodumene to 80% quartz, 40% spodumene to 60% quartz, 60% spodumene to 40% quartz, 80% spodumene to 20% quartz, and 100% spodumene to 0% quartz. The elemental content of these samples was quantitatively measured using an XRF analysis.

The XRF data revealed a linear relationship between the Al content in the non-oxygen component and the proportion of spodumene in the mixture, as shown in Figure A10. The Al content increased from 0.45% in the pure quartz sample (0% spodumene) to 24.61% in the pure spodumene sample (100% spodumene). A calibration curve was constructed by plotting the Al percentage on the $y$-axis against the spodumene percentage on the $x$-axis. The resulting linear equation, $y = 0.2399x - 0.4597$, with an $R^2$ value of 0.9917, shows a strong positive correlation between the spodumene content and the Al percentage.

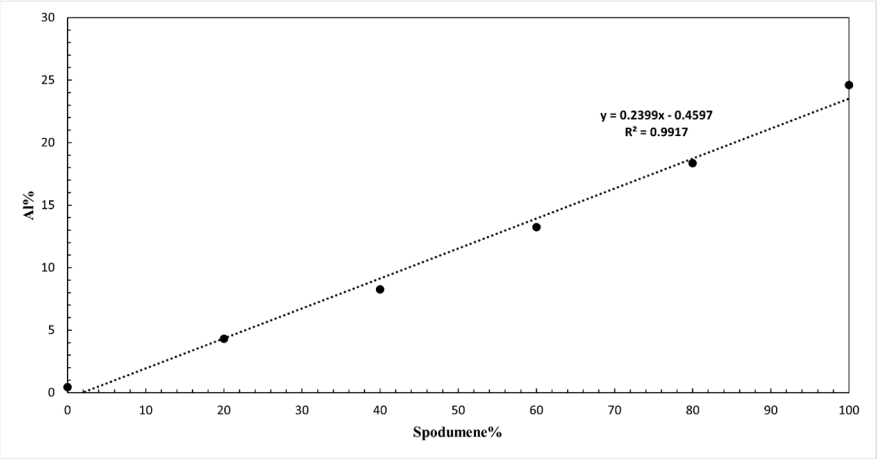


**Figure A10.** Calibration curve for determining the spodumene concentration from the Al content measured by XRF.

This calibration curve can be used to determine the spodumene content of unknown spodumene–quartz mixtures by measuring their Al content, since this curve was constructed for a synthetic mixture produced from a known feed. This method assumes that the Al content is primarily derived from spodumene, reflecting the known compositions of these minerals. For example, consider the calculation for an unknown mixture of spodumene and quartz. For a pure mixture of spodumene and quartz, the major elements detectable by XRF are Si and Al. Given a sample with measured values of Al = 14.92% and Si = 78.1%, the recalculated values for Al and Si, ensuring they sum to 100%, would be Al (%) = 16.04 and Si (%) = 83.96. Using these adjusted values, the spodumene content could be calculated using the calibration curve equation

$$\text{Spodumene content\%} = \frac{(\text{Al\%} + 0.4597)}{0.2399} = \frac{(16.04 + 0.4597)}{0.2399} = 68.76\%$$

By substituting the Al content into the equation, the exact percentage of spodumene in the unknown sample could be determined. It should be emphasised that XRF cannot measure oxygen or lithium, hence the given %Al and %Si represents only the fraction net of oxygen and lithium.

*Appendix A.11. Speciation of (Ca(II)aq) as a Function of pH*

The dissolved calcium ($Ca(II)_{aq}$) will be present as $Ca^{2+}$, $Ca(OH)^+$, or $Ca(OH)_2$, depending on the pH [86]. The adsorption strength of calcium on the surface of the spodumene increases in the following sequence: $Ca^{2+}$, $Ca(OH)^+$, and $Ca(OH)_2$ [86]. At pH 8.5, the concentration of $Ca^{2+}$ is more than 1000 times the concentration of $Ca(OH)^+$, and reduces to 100 times at pH 10.5. At about a pH 12, the concentrations of $Ca^{2+}$, $Ca(OH)^+$, and $Ca(OH)_2$ are about equal. Based on the adsorption strength, $Ca(OH)^+$ is recognised as the active component that most effectively facilitates the adsorption of the carboxylate group ($-COO^-$) and spodumene flotation [86]. The concentration of $Ca(OH)^+$ is related to the pH, so activation using calcium is sensitive to the pH. A similar activation mechanism acts on quartz, though only at high pH levels (pH > 10), as $Ca(OH)^+$ adsorbs onto the negatively charged quartz surface [52,56,63–67]. Spodumene activation primarily occurs between pH 8 and 12, largely due to the presence of $Ca(OH)^+$ [25,87,88].

*Appendix A.12. Effect of Polymer Charge: Chord Length Distributions*

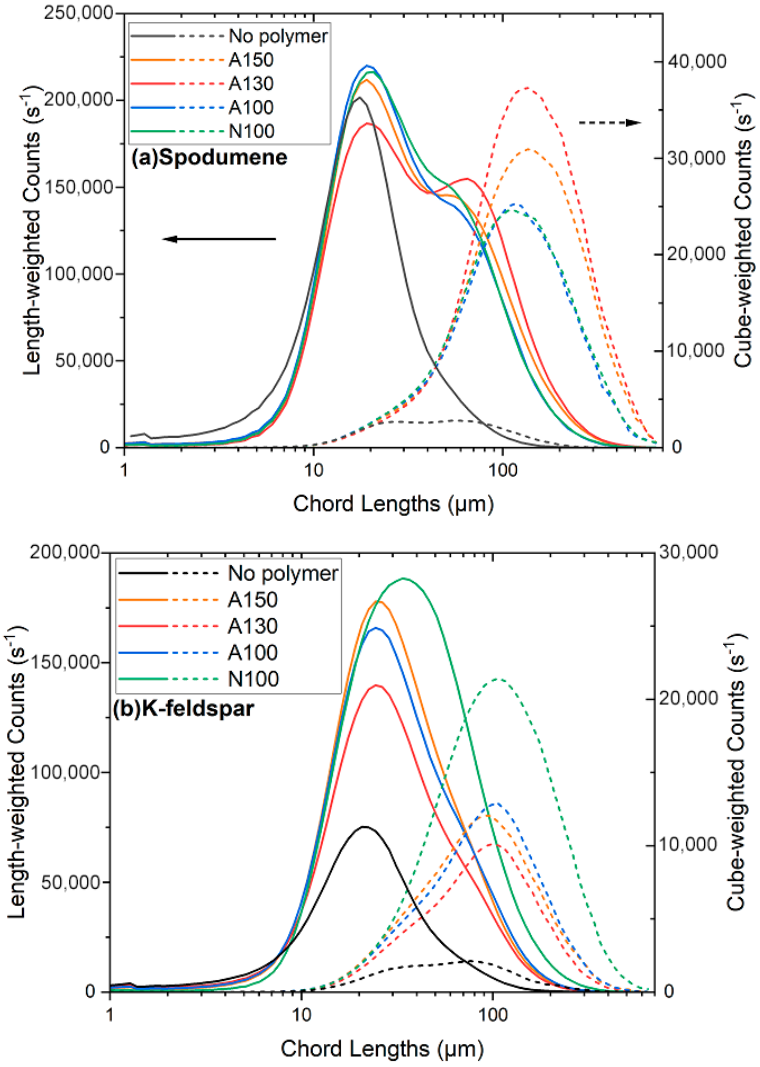


**Figure A11.** *Cont.*

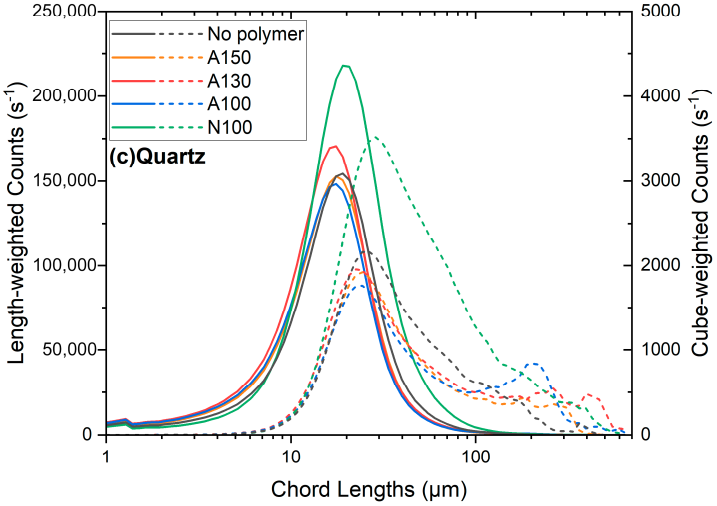


**Figure A11.** Length- and cube-weighted chord lengths measured 5 min after the addition of the polymer at pH 8.5, with a constant calcium concentration of 625 g/t, a constant polymer concentration of 42 g/t, and varying charges of the anionic polymer: (**a**) spodumene, (**b**) K-feldspar, (**c**) quartz. N100 is a non-ionic polymer with a charge density below 2%. (A100, A130, A150) are anionic flocculants of increasing charge density (6.4%, 30%, 58%, respectively).

*Appendix A.13. Effect of Polymer Molecular Weight: Chord Length Distributions*

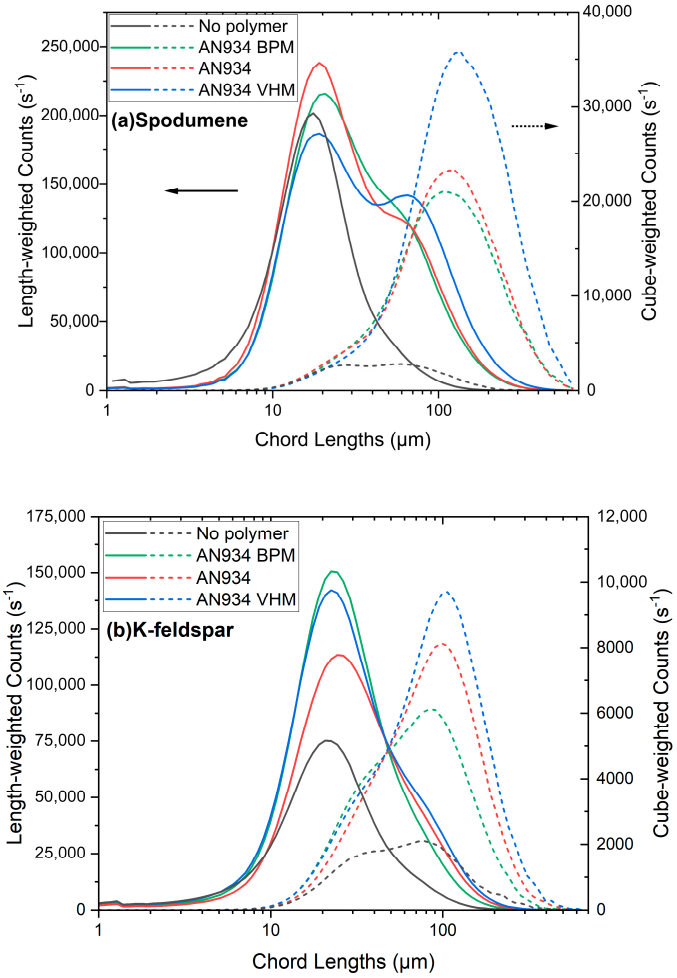


**Figure A12.** *Cont.*

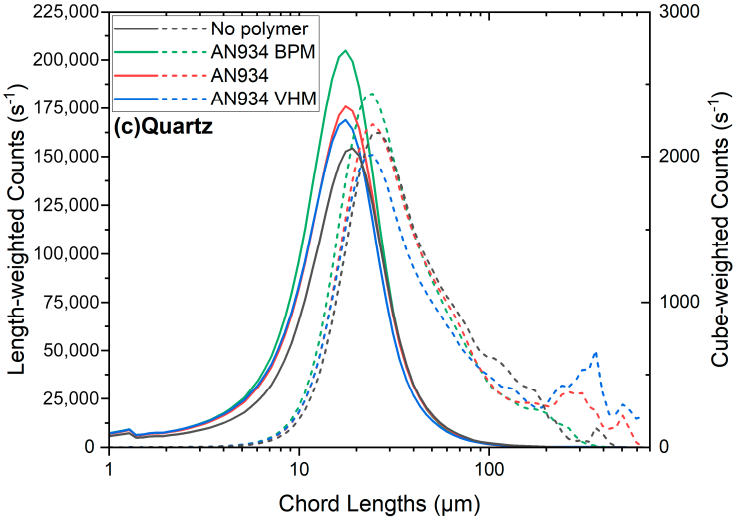


**Figure A12.** Length- and cube-weighted chord lengths measured 5 min after the addition of the polymer at pH 8.5, with a constant calcium concentration of 625 g/t, a constant polymer concentration of 42 g/t, and varying weights of the anionic polymer: (**a**) spodumene, (**b**) K-feldspar, (**c**) quartz. AN934 has a molecular weight of about 6 MDa, AN934 has a molecular weight of about 12 MDa, and AN934 VHM has a molecular weight of about 18 MDa. All the polymers used here contain about a 30% anionic charge.

### *Appendix A.14. Turbidity: Repeat Measurements*

**Table A2.** Tabulated values for the turbidity readings from Figure 8. Selected conditions were repeated; for these results, the values shown represent the average along with the 95% confidence interval.

| | **Polymer Concentration** | **$Ca^{2+}$ Concentration** | | | | | | | |
|---|---|---|---|---|---|---|---|---|---|
| | | **0 g/t** | **312.5 g/t** | **625 g/t** | **1250 g/t** | **2500 g/t** | **5000 g/t** | **10,000 g/t** | **15,000 g/t** |
| Spodumene | 0 g/t | 4925 ± 46 | 4826 ± 54 | 4844 ± 91 | 4849 ± 59 | 4825 ± 62 | 4870 ± 111 | 4567 | 4984 |
| | 21.05 g/t | 4583 | 327 ± 24 | 266 ± 5 | 371 ± 9 | 420 | 552 | 343 | 285 |
| | 42.11 g/t | 4579 | 328 ± 1 | 156 ± 11 | 150 ± 10 | 214 | 287 | 139 | 129 |
| | 63.17 g/t | 4785 | 173 ± 25 | 120 | 94 | 203 | 107 | 56 | 31 |
| | 84.22 g/t | 4589 | 161 | 117 | 150 | 200 | 21 | 216 | 174 |
| | 147.35 g/t | 3489 | 51 | 78 | 200 | 101 | 90 | 97 | 189 |
| | 280.73 g/t | 3456 | 23 | 77 | 142 | 61 | 48 | 64 | 210 |
| K-feldspar | 0 g/t | 5380 ± 59 | 5359 ± 11 | 5466 | 5615 ± 260 | 5448 ± 15 | 5234 | 5364 | 5289 |
| | 21.05 g/t | 5753 ± 321 | 1832 ± 255 | 1127 ± 30 | 574 | 569 | 433 | 260 | 251 |
| | 42.11 g/t | 5852 ± 232 | 2656 ± 314 | 1376 ± 50 | 417 | 564 | 374 | 206 | 300 |
| | 63.17 g/t | 5430 | 2167 ± 395 | 1332 ± 30 | 590 | 355 | 211 | 366 | 136 |
| | 84.22 g/t | 5433 | 2739 | 1167 | 610 | 447 | 401 | 109 | 124 |
| | 147.35 g/t | 5609 | 2300 | 2592 | 1870 | 295 | 460 | 53 | 142 |
| | 280.73 g/t | 5304 | 1672 | 3593 | 2230 | 468 | 892 | 555 | 287 |
| Quartz | 0 g/t | 6434 ± 44 | 6517 ± 170 | 6462 ± 58 | 6430 | 6021 | 6520 | 6302 | 6013 |
| | 21.05 g/t | 6500 | 6485 ± 474 | 6980 ± 490 | 5926 | 5890 | 2425 | 1591 | 833 |
| | 42.11 g/t | 6499 ± 21 | 6355 ± 365 | 6529 | 6540 | 5987 | 3098 | 1873 | 2108 |
| | 63.17 g/t | 6402 ± 163 | 6003 ± 5 | 7080 | 6549 | 5678 | 4629 | 5488 | 6317 |
| | 84.22 g/t | 6293 | 6566 | 6790 | 6578 | 5879 | 4559 | 3238 | 4268 |
| | 147.35 g/t | 6433 | 5070 | 6674 | 6536 | 5709 | 6429 | 5446 | 4966 |
| | 280.73 g/t | 6200 | 6000 | 4777 | 5924 | 5898 | 6076 | 6084 | 4501 |

## References


1. Sahoo, S.K.; Tripathy, S.K.; Nayak, A.; Hembrom, K.; Dey, S.; Rath, R.; Mohanta, M. Beneficiation of lithium bearing pegmatite rock: A review. *Miner. Process. Extr. Metall. Rev.* **2024**, *45*, 1–27. [CrossRef]
2. Dessemond, C.; Lajoie-Leroux, F.; Soucy, G.; Laroche, N.; Magnan, J.-F. Spodumene: The lithium market, resources and processes. *Minerals* **2019**, *9*, 334. [CrossRef]
3. Kundu, T.; Rath, S.S.; Das, S.K.; Parhi, P.K.; Angadi, S.I. Recovery of lithium from spodumene-bearing pegmatites: A comprehensive review on geological reserves, beneficiation, and extraction. *Powder Technol.* **2023**, *415*, 118142. [CrossRef]
4. Salakjani, N.K.; Singh, P.; Nikoloski, A.N. Production of lithium—A literature review part 1: Pretreatment of spodumene. *Miner. Process. Extr. Metall. Rev.* **2020**, *41*, 335–348. [CrossRef]
5. Ruberti, M. Pathways to Greener Primary Lithium Extraction for a Really Sustainable Energy Transition: Environmental Challenges and Pioneering Innovations. *Sustainability* **2024**, *17*, 160. [CrossRef]
6. Nolan, B. Spodumene: Australia's Lithium Mineral Hero: Commonwealth Scientific and Industrial Research Organisation (CSIRO). 2025. Available online: https://www.csiro.au/en/news/All/Articles/2025/March/Spodumene-Australias-lithium-mineral-hero (accessed on 1 May 2025).
7. Li, Z.; Perry, C. Spodumene and Lithium Salts Prices: Exploring the Connection: Fastmarkets. 2025. Available online: https://www.fastmarkets.com/insights/relationship-spodumene-lithium-salts-prices/ (accessed on 1 April 2025).
8. Kawenski Cook, B.; Aghamirian, M.; Gibson, C.E. Optimization of spodumene flotation with a fatty acid collector. *Miner. Eng.* **2023**, *204*, 108412. [CrossRef]
9. Menéndez, M.; Vidal, J.; Toraño, J.; Gent, M. Optimisation of spodumene flotation. *Eur. J. Miner. Process. Environ. Prot.* **2004**, *4*, 130–135.
10. Hoang, D.H.; Ebert, D.; Möckel, R.; Rudolph, M. Impact of Sodium Hexametaphosphate on the Flotation of Ultrafine Magnesite from Dolomite-Rich Desliming Tailings. *Minerals* **2021**, *11*, 499. [CrossRef]
11. Lynch, A.J.; Johnson, N.; Manlapig, E.; Thorne, C. *Mineral and Coal Flotation Circuits: Their simulation and Control*; Elsevier Science Ltd.: Amsterdam, The Netherlands, 1981.
12. Miettinen, T.; Ralston, J.; Fornasiero, D. The limits of fine particle flotation. *Miner. Eng.* **2010**, *23*, 420–437. [CrossRef]
13. Yin, X.; Gupta, V.; Du, H.; Wang, X.; Miller, J.D. Surface charge and wetting characteristics of layered silicate minerals. *Adv. Colloid Interface Sci.* **2012**, *179–182*, 43–50. [CrossRef]
14. Laskowski, J. *Particle-Bubble Attachment in Flotation*; Inist-CNRS: Nancy, France, 1974; Volume 6, pp. 223–235.
15. Ralston, J. The influence of particle size and contact angle in flotation. In *Developments in Mineral Processing*; Elsevier: Amsterdam, The Netherlands, 1992; Volume 12, pp. 203–224.
16. Trahar, W.J. A rational interpretation of the role of particle size in flotation. *Int. J. Miner. Process.* **1981**, *8*, 289–327. [CrossRef]
17. Fosu, A.Y.; Kanari, N.; Bartier, D.; Hodge, H.; Vaughan, J.; Chagnes, A. Physico-Chemical Characteristics of Spodumene Concentrate and Its Thermal Transformations. *Materials* **2021**, *14*, 7423. [CrossRef]
18. Xiang, G.; Tao, L.; Sun, W.; Xu, S.; Gao, Z. Mechanisms for the selective separation of spodumene from feldspar by sodium N-oleoylsarcosinate as an efficient collector. *Appl. Surf. Sci.* **2023**, *636*, 157821. [CrossRef]
19. Bulatovic, S.M. *Handbook of Flotation Reagents: Chemistry, Theory and Practice: Volume 1: Flotation of Sulfide Ores*; Elsevier: Amsterdam, The Netherlands, 2007; Volume 2, p. 87.
20. Tadesse, B.; Makuei, F.; Albijanic, B.; Dyer, L. The beneficiation of lithium minerals from hard rock ores: A review. *Miner. Eng.* **2019**, *131*, 170–184. [CrossRef]
21. Jie, Z.; Weiqing, W.; Jing, L.; Yang, H.; Qiming, F.; Hong, Z. Fe (III) as an activator for the flotation of spodumene, albite, and quartz minerals. *Miner. Eng.* **2014**, *61*, 16–22. [CrossRef]
22. Liu, W.; Zhang, S.; Wang, W.; Zhang, J.; Yan, W.; Deng, J.; Feng, Q.; Huang, Y. The effects of Ca (II) and Mg (II) ions on the flotation of spodumene using NaOL. *Miner. Eng.* **2015**, *79*, 40–46. [CrossRef]
23. Xu, L.; Hu, Y.; Wu, H.; Tian, J.; Liu, J.; Gao, Z.; Wang, L. Surface crystal chemistry of spodumene with different size fractions and implications for flotation. *Sep. Purif. Technol.* **2016**, *169*, 33–42. [CrossRef]
24. Wang, Y.-h.; Yu, F.-s. Effects of metallic ions on the flotation of spodumene and beryl. *J. China Univ. Min. Technol.* **2007**, *17*, 35–39. [CrossRef]
25. Tian, J.; Xu, L.; Wu, H.; Fang, S.; Deng, W.; Peng, T.; Sun, W.; Hu, Y. A novel approach for flotation recovery of spodumene, mica and feldspar from a lithium pegmatite ore. *J. Clean. Prod.* **2018**, *174*, 625–633. [CrossRef]
26. Tian, M.; Gao, Z.; Sun, W.; Han, H.; Sun, L.; Hu, Y. Activation role of lead ions in benzohydroxamic acid flotation of oxide minerals: New perspective and new practice. *J. Colloid Interface Sci.* **2018**, *529*, 150–160. [CrossRef]
27. Lu, S.; Song, S. Hydrophobic interaction in flocculation and flotation 1. Hydrophobic flocculation of fine mineral particles in aqueous solution. *Colloids Surf.* **1991**, *57*, 49–60. [CrossRef]
28. Subrahmanyam, T.V.; Forssberg, K.S.E. Fine particles processing: Shear-flocculation and carrier flotation—A review. *Int. J. Miner. Process.* **1990**, *30*, 265–286. [CrossRef]

29. Forbes, E. Shear, selective and temperature responsive flocculation: A comparison of fine particle flotation techniques. *Int. J. Miner. Process.* **2011**, *99*, 1–10. [CrossRef]
30. Ng, W.S.; Connal, L.A.; Forbes, E.; Mohanarangam, K.; Franks, G.V. In situ investigation of aggregate sizes formed using thermo-responsive polymers: Effect of temperature and shear. *J. Colloid Interface Sci.* **2017**, *494*, 139–152. [CrossRef] [PubMed]
31. Ng, W.S.; Sonsie, R.; Forbes, E.; Franks, G.V. Flocculation/flotation of hematite fines with anionic temperature-responsive polymer acting as a selective flocculant and collector. *Miner. Eng.* **2015**, *77*, 64–71. [CrossRef]
32. Franks, G.V.; Li, H.; O'Shea, J.-P.; Qiao, G.G. Temperature responsive polymers as multiple function reagents in mineral processing. *Adv. Powder Technol.* **2009**, *20*, 273–279. [CrossRef]
33. Li, M.; Xiang, Y.; Chen, T.; Gao, X.; Liu, Q. Separation of ultra-fine hematite and quartz particles using asynchronous flocculation flotation. *Miner. Eng.* **2021**, *164*, 106817. [CrossRef]
34. Zhang, J.; Sun, W.; Gao, Z.; Niu, F.; Wang, L.; Zhao, Y.; Gao, Y. Selective Flocculation Separation of Fine Hematite from Quartz Using a Novel Grafted Copolymer Flocculant. *Minerals* **2018**, *8*, 227. [CrossRef]
35. Zhou, H.-P.; Hu, J.; Zhang, Y.-B.; Cao, Y.-J.; Luo, X.-P.; Tang, X.-K. Effectively enhancing recovery of fine spodumene via aggregation flotation. *Rare Met.* **2020**, *39*, 316–326. [CrossRef]
36. Gao, J.; Sun, W.; Lyu, F. Understanding the activation mechanism of Ca2+ ion in sodium oleate flotation of spodumene: A new perspective. *Chem. Eng. Sci.* **2021**, *244*, 116742. [CrossRef]
37. Huber, K. Calcium-induced shrinking of polyacrylate chains in aqueous solution. *J. Phys. Chem.* **2002**, *97*, 9825–9830. [CrossRef]
38. Atesok, G.; Somasundaran, P.; Morgan, L. Adsorption properties of $Ca^{2+}$ on Na-kaolinite and its effect on flocculation using polyacrylamides. *Colloids Surf.* **1988**, *32*, 127–138. [CrossRef]
39. Caskey, J.A.; Primus, R.J. The effect of anionic polyacrylamide molecular conformation and configuration on flocculation effectiveness. *Environ. Prog.* **2006**, *5*, 98–103. [CrossRef]
40. Peng, F.F.; Di, P. Effect of Multivalent Salts—Calcium and Aluminum on the Flocculation of Kaolin Suspension with Anionic Polyacrylamide. *J. Colloid Interface Sci.* **1994**, *164*, 229–237. [CrossRef]
41. de Medeiros, R.B.; Thomas, C.A.; Franks, G.V. Selective aggregation of fine copper minerals using charged polyacrylamides. *Colloids Surf. A Physicochem. Eng. Asp.* **2024**, 134396. [CrossRef]
42. Eardley, J.C.; Thomas, C.A.; Franks, G.V. Selective aggregation of hematite from quartz using charged polyacrylamides: In-situ sizing. *Miner. Eng.* **2024**, *217*, 108924. [CrossRef]
43. Camp, T.R. Velocity gradients and internal work in fluid motion. *J. Boston Soc. Civ. Eng.* **1943**, *30*, 219–230.
44. Pandit, A.V.; Ranade, V.V. Chord length distribution to particle size distribution. *AIChE J.* **2016**, *62*, 4215–4228. [CrossRef]
45. Wynn, E.J.W. Relationship between particle-size and chord-length distributions in focused beam reflectance measurement: Stability of direct inversion and weighting. *Powder Technol.* **2003**, *133*, 125–133. [CrossRef]
46. Chen, Y.; Zhou, J.; He, G.; Hu, H.; Liu, C.; Yang, J.; Lyu, X. The effect of Al (III) and Fe (III) ions on the flotation behavior of Kfeldspar with sodium oleate as the collector. *Physicochem. Probl. Miner. Process.* **2023**, *59*, 174724.
47. Fan, G.; Wang, L.; Cao, Y.; Li, C. Collecting Agent–Mineral Interactions in the Reverse Flotation of Iron Ore: A Brief Review. *Minerals* **2020**, *10*, 681. [CrossRef]
48. Yukselen-Aksoy, Y.; Kaya, A. A study of factors affecting on the zeta potential of kaolinite and quartz powder. *Environ. Earth Sci.* **2010**, *62*, 697–705. [CrossRef]
49. Vidyadhar, A.; Kumari, N.; Bhagat, R. Flotation of quartz and hematite: Adsorption mechanism of mixed cationic/anionic collector systems. In Proceedings of the XXVI International Mineral Processing Congress (IMPC-2012), New Delhi, India, 24–28 September 2012.
50. Franks, G.V. Zeta Potentials and Yield Stresses of Silica Suspensions in Concentrated Monovalent Electrolytes: Isoelectric Point Shift and Additional Attraction. *J. Colloid Interface Sci.* **2002**, *249*, 44–51. [CrossRef] [PubMed]
51. Yu, F.S.; Wang, Y.H.; Wang, J.M.; Xie, Z.F. Invetigation on different behavior and mechanism of Ca2+, Fe3+ adsorption on spodumente surface. *Physicochem. Probl. Miner. Process.* **2014**, *50*, 535–550. [CrossRef]
52. Ozkan, A.; Ucbeyiay, H.; Duzyol, S. Comparison of stages in oil agglomeration process of quartz with sodium oleate in the presence of Ca (II) and Mg (II) ions. *J. Colloid Interface Sci.* **2009**, *329*, 81–88. [CrossRef]
53. Owens, G.J.; Singh, R.K.; Foroutan, F.; Alqaysi, M.; Han, C.-M.; Mahapatra, C.; Kim, H.-W.; Knowles, J.C. Sol–Gel based materials for biomedical applications. *Prog. Mater. Sci.* **2016**, *77*, 1–79. [CrossRef]
54. Hao, H.; Li, L.; Yuan, Z.; Liu, J. Molecular arrangement of starch, Ca2+ and oleate ions in the siderite-hematite-quartz flotation system. *J. Mol. Liq.* **2018**, *254*, 349–356. [CrossRef]
55. Cooke, S.R.B. The Flotation of Quartz Using Calcium Ion as Activator. *Trans. Am. Inst. Min. Metall. Eng.* **1949**, *184*, 306–309.
56. Wang, L.; Wang, G.; Ge, P.; Sun, W.; Tang, H.; Hu, W. Activation mechanisms of quartz flotation with calcium ions and cationic/anionic mixed collectors under alkalescent conditions. *Colloids Surf. A Physicochem. Eng. Asp.* **2022**, *632*, 127771. [CrossRef]
57. Hunter, R.J. *Foundations of Colloid Science*, 2nd ed.; Oxford University Press: Oxford, UK, 2001.
58. Rhodes, M.J. *Introduction to Particle Technology*, 2nd ed.; John Wiley & Sons, Ltd.: Chichester, UK, 2008.

59. Ma, Z.; Tian, J.; Xu, L.; Li, C.; Wang, D.; Xue, K. Comparison of surface physicochemical properties of spodumene and feldspar using different grinding media: Implications for flotation separation. *Miner. Eng.* **2024**, *216*, 108878. [CrossRef]
60. Moon, K.S.; Fuerstenau, D.W. Surface crystal chemistry in selective flotation of spodumene ($LiAl[SiO_3]_2$) from other aluminosilicates. *Int. J. Miner. Process.* **2003**, *72*, 11–24. [CrossRef]
61. Cui, M.; Li, Y.; Zhang, Y.; Zhu, G.; Wang, Y.; Lu, D.; Zheng, X. The relationship between spodumene surface pretreatment and flotation behavior: A review. *Sep. Sci. Technol.* **2024**, *59*, 464–480. [CrossRef]
62. Xie, R.; Zhu, Y.; Liu, J.; Li, Y. Effects of metal ions on the flotation separation of spodumene from feldspar and quartz. *Miner. Eng.* **2021**, *168*, 106931. [CrossRef]
63. Ruan, Y.; Zhang, Z.; Luo, H.; Xiao, C.; Zhou, F.; Chi, R. Effects of Metal Ions on the Flotation of Apatite, Dolomite and Quartz. *Minerals* **2018**, *8*, 141. [CrossRef]
64. Luo, A.; Chen, J. Effect of hydration and hydroxylation on the adsorption of metal ions on quartz surfaces: DFT study. *Appl. Surf. Sci.* **2022**, *595*, 153553. [CrossRef]
65. Wang, X.; Liu, W.; Duan, H.; Wang, B.; Han, C.; Wei, D. The adsorption mechanism of calcium ion on quartz (101) surface: A DFT study. *Powder Technol.* **2018**, *329*, 158–166. [CrossRef]
66. Feng, Q.; Wen, S.; Zhao, W.; Chen, Y. Effect of calcium ions on adsorption of sodium oleate onto cassiterite and quartz surfaces and implications for their flotation separation. *Sep. Purif. Technol.* **2018**, *200*, 300–306. [CrossRef]
67. Luo, X.; Lin, Q.; Wang, Y.; Tian, M.; Lai, H.; Bai, S.; Zhou, Y. New insights into the activation mechanism of calcium species to quartz: ToF-SIMS and AFM investigation. *Miner. Eng.* **2020**, *153*, 106398. [CrossRef]
68. Cao, M.; Bu, H.; Li, S.; Meng, Q.; Gao, Y.; Ou, L. Impact of differing water hardness on the spodumene flotation. *Miner. Eng.* **2021**, *172*, 107159. [CrossRef]
69. Amarante, M.M.; de Sousa, A.B.; Leite, M.M. Processing a spodumene ore to obtain lithium concentrates for addition to glass and ceramic bodies. *Miner. Eng.* **1999**, *12*, 433–436. [CrossRef]
70. Tian, J.; Xu, L.; Deng, W.; Jiang, H.; Gao, Z.; Hu, Y. Adsorption mechanism of new mixed anionic/cationic collectors in a spodumene-feldspar flotation system. *Chem. Eng. Sci.* **2017**, *164*, 99–107. [CrossRef]
71. Xu, L.; Jiao, F.; Jia, W.; Pan, Z.; Hu, C.; Qin, W. Selective flotation separation of spodumene from feldspar using mixed anionic/nonionic collector. *Colloids Surf. A Physicochem. Eng. Asp.* **2020**, *594*, 124605. [CrossRef]
72. Xu, L.; Hu, Y.; Tian, J.; Wu, H.; Yang, Y.; Zeng, X.; Wang, Z.; Wang, J. Selective flotation separation of spodumene from feldspar using new mixed anionic/cationic collectors. *Miner. Eng.* **2016**, *89*, 84–92. [CrossRef]
73. Wang, Y.; Zhu, G.; Yu, F.; Lu, D.; Wang, L.; Zhao, Y.; Zheng, H. Improving spodumene flotation using a mixed cationic and anionic collector. *Physicochem. Probl. Miner. Process.* **2018**, *54*, 567–577. [CrossRef]
74. Xie, R.; Zhu, Y.; Li, Y.; Han, Y. Flotation behavior and mechanism of a new mixed collector on separation of spodumene from feldspar. *Colloids Surf. A Physicochem. Eng. Asp.* **2020**, *599*, 124932. [CrossRef]
75. Xie, R.; Zhu, Y.; Liu, J.; Li, Y. The flotation behavior and adsorption mechanism of a new cationic collector on the separation of spodumene from feldspar and quartz. *Sep. Purif. Technol.* **2021**, *264*, 118445. [CrossRef]
76. Wu, H.; Tian, J.; Xu, L.; Fang, S.; Zhang, Z.; Chi, R. Flotation and adsorption of a new mixed anionic/cationic collector in the spodumene-feldspar system. *Miner. Eng.* **2018**, *127*, 42–47. [CrossRef]
77. Zhu, G.; Wang, Y.; Wang, X.; Yu, F.; Miller, J.D. States of coadsorption for oleate and dodecylamine at selected spodumene surfaces. *Colloids Surf. A Physicochem. Eng. Asp.* **2018**, *558*, 313–321. [CrossRef]
78. Shu, K.; Xu, L.; Wu, H.; Xu, Y.; Luo, L.; Yang, J.; Tang, Z.; Wang, Z. In Situ Adsorption of Mixed Anionic/Cationic Collectors in a Spodumene–Feldspar Flotation System: Implications for Collector Design. *Langmuir* **2020**, *36*, 8086–8099. [CrossRef]
79. Xie, R.; Zhu, Y.; Liu, J.; Li, Y. Flotation behavior and mechanism of α-bromododecanoic acid as collector on the flotation separation of spodumene from feldspar and quartz. *J. Mol. Liq.* **2021**, *336*, 116303. [CrossRef]
80. Wang, Y.; Zhu, G.; Zhang, L.; Lu, D.; Wang, L.; Zhao, Y.; Zheng, H. Surface dissolution of spodumene and its role in the flotation concentration of a spodumene ore. *Miner. Eng.* **2018**, *125*, 120–125. [CrossRef]
81. Ma, Z.; Xu, L.; Guo, W.; Wang, D.; Xue, K. Effects of alkali pretreatment on the flotation of spodumene and feldspar. *Miner. Eng.* **2024**, *210*, 108676. [CrossRef]
82. Zhu, G.; Zhao, Y.; Zheng, X.; Wang, Y.; Zheng, H.; Lu, D. Understanding the role of sodium hydroxide in the selective flotation separation of spodumene from feldspar and quartz. *Miner. Eng.* **2020**, *159*, 106648. [CrossRef]
83. Wang, Y.; Sun, N.; Chu, H.; Zheng, X.; Lu, D.; Zheng, H. Surface dissolution behavior and its influences on the flotation separation of spodumene from silicates. *Sep. Sci. Technol.* **2021**, *56*, 1407–1417. [CrossRef]
84. Guo, W.; Fang, J.; Liu, M.; Li, Y.; Wang, D.; Xue, K.; Tian, J.; Shu, K.; Wang, Z.; Xie, L.; et al. Ultrasound-assisted alkali pretreatment enhances the flotation of spodumene. *Colloids Surf. A Physicochem. Eng. Asp.* **2025**, *716*, 136685. [CrossRef]
85. Dai, L.; Feng, B.; Zhang, L.; Chen, Y.; Bayoundoula, J. Selective flotation separation of spodumene and quartz with carboxylated chitosan as depressant. *Miner. Eng.* **2023**, *203*, 108343. [CrossRef]

86. Yongbing, Z.; Hepeng, Z.; Yijun, C.; Xianping, L.; Fanxin, X.; Boyuan, Z.; Siqi, Y. Activation mechanism of calcium hydrolysate on the spodumene surface and its effect on the adsorption of collector. *Miner. Eng.* **2021**, *174*, 107221. [CrossRef]
87. Filippov, L.; Farrokhpay, S.; Lyo, L.; Filippova, I. Spodumene Flotation Mechanism. *Minerals* **2019**, *9*, 372. [CrossRef]
88. Retamal, J.I.; Robles, P.A.; Quezada, G.R.; Jeldres, R.I. Molecular Design and Spodumene Flotation—A Review. *Int. J. Mol. Sci.* **2024**, *25*, 3227. [CrossRef]